











Towards species-level forecasts of drought-induced tree mortality risk

Martin G. De Kauwe¹ , Manon E. B. Sabot^{2,3} , Belinda E. Medlyn⁴ , Andrew J. Pitman^{2,3} ,
Patrick Meir⁵ , Lucas A. Cernusak⁶ , Rachael V. Gallagher⁴ , Anna M. Ukkola^{2,3} , Sami W. Rifai^{2,3}  and
Brendan Choat⁴ 

¹School of Biological Sciences, University of Bristol, Bristol, BS8 1TQ, UK; ²ARC Centre of Excellence for Climate Extremes, Sydney, NSW 2052, Australia; ³Climate Change Research Centre, University of New South Wales, Sydney, NSW 2052, Australia; ⁴Hawkesbury Institute for the Environment, Western Sydney University, Locked Bag 1797, Penrith, NSW 2751, Australia; ⁵School of Geosciences, The University of Edinburgh, Edinburgh, EH9 3FF, UK; ⁶College of Science and Engineering, James Cook University, Cairns, Qld 4878, Australia

Summary

Author for correspondence:
Martin G. De Kauwe
Email: m.dekauwe@bristol.ac.uk

Received: 8 December 2021
Accepted: 28 March 2022

New Phytologist (2022) **235**: 94–110
doi: 10.1111/nph.18129

Key words: Australia, cavitation resistance, drought tolerance, land surface model, plant hydraulics, species.

- Predicting species-level responses to drought at the landscape scale is critical to reducing uncertainty in future terrestrial carbon and water cycle projections.
- We embedded a stomatal optimisation model in the Community Atmosphere Biosphere Land Exchange (CABLE) land surface model and parameterised the model for 15 canopy dominant eucalypt tree species across South-Eastern Australia (mean annual precipitation range: 344–1424 mm yr⁻¹). We conducted three experiments: applying CABLE to the 2017–2019 drought; a 20% drier drought; and a 20% drier drought with a doubling of atmospheric carbon dioxide (CO₂).
- The severity of the drought was highlighted as for at least 25% of their distribution ranges, 60% of species experienced leaf water potentials beyond the water potential at which 50% of hydraulic conductivity is lost due to embolism. We identified areas of severe hydraulic stress within-species' ranges, but we also pinpointed resilience in species found in predominantly semiarid areas. The importance of the role of CO₂ in ameliorating drought stress was consistent across species.
- Our results represent an important advance in our capacity to forecast the resilience of individual tree species, providing an evidence base for decision-making around the resilience of restoration plantings or net-zero emission strategies.

Introduction

Droughts, including the co-occurrence of droughts and heatwaves (Mueller & Seneviratne, 2012; Reichstein *et al.*, 2013), have emerged as one of the principal threats to the function of terrestrial ecosystems and are projected to worsen into the future in some regions (Ridder *et al.*, 2020; Ukkola *et al.*, 2020). These 'hotter droughts' – due both to an increase in heatwaves and a background warming of the climate – have been identified as a key driver in reducing plant productivity (Zscheischler *et al.*, 2014), growth (Julio Camarero *et al.*, 2018; Scharnweber *et al.*, 2020) and the terrestrial carbon sink (Yang *et al.*, 2018; Green *et al.*, 2019). Ultimately, if droughts result in widespread species dieback (Mantgem *et al.*, 2009; Peng *et al.*, 2011; Mitchell *et al.*, 2014), they may lead to sustained changes in biodiversity and community composition (Slik, 2004; Nepstad *et al.*, 2007; Anderegg *et al.*, 2013), altering land–atmosphere feedbacks (Swann *et al.*, 2018) on seasonal to decadal timescales. To develop a predictive framework and better understand the impacts and implications of changes in the timing, severity and spatial extent of climatic extremes, we need to combine insights

across scales (McDowell *et al.*, 2016), including field ecology (Rowland *et al.*, 2015), remote sensing (Bastos *et al.*, 2021), modelling and climate science (Williams *et al.*, 2020).

Efforts towards understanding the physiological controls of drought-induced mortality (McDowell *et al.*, 2008; Choat *et al.*, 2018; Hammond *et al.*, 2019) are set against a background of widespread reports of dieback due to drought (Allen *et al.*, 2015). Significant progress in our understanding has been enabled by experimental manipulations (Duan *et al.*, 2013; Li *et al.*, 2018; Venturas *et al.*, 2018; Ruehr *et al.*, 2019), field-based surveys and syntheses (Martin-StPaul *et al.*, 2017; Peters *et al.*, 2021) and international coordinated networks (e.g. Drought-Net). More recently, modelling efforts (Bonan *et al.*, 2014; Xu *et al.*, 2016; Sperry *et al.*, 2017; Dewar *et al.*, 2018; Kennedy *et al.*, 2019; Eller *et al.*, 2020; Sabot *et al.*, 2020) have emerged that leverage more mechanistic representations of plant hydraulics, allowing us to scale up our understanding and make landscape-scale predictions (De Kauwe *et al.*, 2020). It is worth reflecting however, that models included in the latest Coupled Model Intercomparison Project (CMIP6) and the Global Carbon Budget (Friedlingstein *et al.*, 2020) lack these recent model advances,

leading to systematic biases in model predictions as water becomes limiting (Ukkola *et al.*, 2016a; Trugman *et al.*, 2018; Humphrey *et al.*, 2021; Teckentrup *et al.*, 2021). To project how species responses to drought affect the land carbon sink, land–atmosphere feedbacks and shifts in species' ranges, we need to incorporate a greater diversity of plant strategies into land surface models (LSMs) and global dynamic vegetation models (De Kauwe *et al.*, 2015a). Ultimately, robust predictions of ecosystem resilience to droughts and heatwaves require an understanding of species' capacities to persist, an understanding of recovery processes/timescales, and the capacity to accommodate interactions with other disturbance agents (i.e. fire; Nolan *et al.*, 2020 and/or insects and pathogens; Trowbridge *et al.*, 2021).

One emerging challenge is how to better connect hydraulics models to observations, particularly as applications of plant hydraulic formulations are applied at larger scales (regional to global). Two contrasting paradigms exist: bottom-up and top-down approaches. Bottom-up approaches have attempted to use modelling to scale up, either by linking empirical thresholds derived in the field to water deficit simulated by models (Anderegg *et al.*, 2015), or by parameterising 'target' species (Sperry *et al.*, 2019; De Kauwe *et al.*, 2020); few have simulated explicit species responses (but please refer to Petit-Cailleux *et al.*, 2021). None of these bottom-up approaches lend themselves to simple incorporation in LSMs used in CMIP6-type initiatives, which instead rely on top-down approaches that group vegetation into plant functional types (PFTs; please refer to Anderegg *et al.* (2022) for a discussion of approaches to capture plant diversity within models). By contrast, top-down approaches could conceivably be parameterised using satellite data. However recent studies (Konings & Gentine, 2017; Liu *et al.*, 2021a) have shown diversity in hydraulics traits (both within and among species) do not readily translate into model PFTs, which may preclude their widespread application in LSMs (Kennedy *et al.*, 2019).

Here, our goal was to advance our capacity to assess tree mortality from a species perspective (bottom-up). De Kauwe *et al.* (2020) previously added a plant hydraulics scheme to Australia's LSM, Community Atmosphere Biosphere Land Exchange (CABLE) and parameterised the model for five broad vegetation types to identify vulnerability to drought. Extending this approach at the species level is challenging because it requires 10 hydraulic parameters per species (e.g. cuticular conductance, leaf/stem capacitance, sapwood density, etc.), which are hard to obtain outside of experimental conditions. Consequently, in this study, we embed a simplified stomatal optimisation model (Sabot *et al.*, 2020) into CABLE that only relies on three hydraulic parameters. We parameterised CABLE for 15 canopy dominant eucalypt tree species (Table 1) originating from a broad precipitation gradient across South-Eastern Australia (mean annual precipitation range: 344–1424 mm yr⁻¹). Between 2017 and 2020, South-Eastern Australia experienced one of the hottest (Abram *et al.*, 2021) and most intense droughts on record (Bureau of Meteorology, 2020), culminating in canopy dieback (Nolan *et al.*, 2021) and record-breaking wildfires (Nolan *et al.*, 2020). We used this period to determine which eucalypt species was most vulnerable to hydraulic drought mortality. Finally, we asked how a future more intense drought and an increase in atmospheric carbon dioxide ([CO₂]) would change predictions of species vulnerability.

Materials and Methods

2017–2020 Drought

Although the winter and spring of 2016 were wet, dry conditions began across Australia in 2017. Across the Murray–Darling basin, rainfall was substantially below average during 2017–2020 and in some regions of South-Eastern Australia it was the lowest on record (Supporting Information Fig. S1).

Table 1 Summary of hydraulic trait parameter values.

Species	<i>b</i> (MPa)	<i>c</i> (–)	<i>P</i> ₁₂ (MPa)	<i>P</i> ₅₀ (MPa)	<i>P</i> ₈₈ (MPa)	Reference
<i>E. blakelyi</i>	5.03	3.36	–2.72	–4.51	–6.12	Li <i>et al.</i> (2018)
<i>E. camaldulensis</i>	4.10	4.35	–2.56	–3.77	–4.15	Franks <i>et al.</i> (1995)
<i>E. crebra</i>	5.52	3.08	–2.83	–4.90	–6.41	Bourne <i>et al.</i> (2017)
<i>E. dunnii</i>	5.56	3.06	–2.84	–4.93	–8.44	Bourne <i>et al.</i> (2017)
<i>E. globulus</i>	2.55	8.30	–1.99	–2.44	–7.48	Barotto <i>et al.</i> (2016)
<i>E. grandis</i>	3.58	5.29	–2.43	–3.34	–4.94	Li <i>et al.</i> (2018) Bourne <i>et al.</i> (2017)
<i>E. largiflorens</i>	8.28	3.25	–4.40	–7.40	–9.95	Li <i>et al.</i> (2018)
<i>E. macrorhyncha</i>	4.40	3.95	–2.61	–4.01	–5.95	Li <i>et al.</i> (2018)
<i>E. melliodora</i>	5.67	3.02	–2.87	–5.02	–6.65	Li <i>et al.</i> (2018)
<i>E. obliqua</i>	2.73	7.67	–2.08	–2.60	–3.64	Pritzkow <i>et al.</i> (2020)
<i>E. populnea</i>	6.41	2.86	–3.12	–5.64	–7.70	Li <i>et al.</i> (2018)
<i>E. saligna</i>	3.65	5.14	–2.45	–3.40	–5.16	Bourne <i>et al.</i> (2017)
<i>E. sideroxydon</i>	4.54	3.79	–2.64	–4.12	–5.30	Li <i>et al.</i> (2018)
<i>E. tereticornis</i>	4.36	3.99	–2.61	–3.98	–5.70	Bourne <i>et al.</i> (2017)
<i>E. viminalis</i>	3.36	5.80	–2.35	–3.15	–4.43	Li <i>et al.</i> (2018)

b(MPa) and *c* (unitless) are sensitivity and shape parameters of the plant hydraulic vulnerability curve. *P*₁₂, *P*₅₀ and *P*₈₈ are the water potential inducing a 12%, 50% and 88% loss in hydraulic function, respectively. Note, the value for *Eucalyptus grandis* represents the average trait values taken from the two cited references. [Correction added after first publication 22 April 2022: a reference in the table has been corrected.]

A range of drought definitions exist (Cook *et al.*, 2018). Here we only consider the meteorological drought (a deficit of long-term rainfall) of 2017–2020 in South-Eastern Australia and the resulting impact on the vegetation (ecological drought), as simulated by the CABLE plant hydraulics scheme (please refer to below). Fig. 1 shows the 6-month Standardised Precipitation Index (SPI; McKee *et al.*, 1993) calculated from the Bureau of Meteorology's Australian Water Availability Project (AWAP) (Jones *et al.*, 2009) precipitation data. A 6-month SPI represents a 'medium-term' precipitation deficit, often associated with anomalous streamflow and reservoir levels. Fig. 1 shows extensive areas where the SPI exceeded -0.5 and some regions of southern Victoria where it exceeded -1.0 . In short, South-Eastern Australia was subject to widespread and significant meteorological drought during the study period.

Model description

CABLE is the land surface scheme used in the Australian Community Climate Earth System Simulator (ACCESS, please refer to

<http://www.accessimulator.org.au>; Kowalczyk *et al.*, 2006). CABLE can be run offline using prescribed meteorological forcing (Wang *et al.*, 2011; De Kauwe *et al.*, 2015b; Ukkola *et al.*, 2016b; Decker *et al.*, 2017; Haverd *et al.*, 2018), or fully coupled (Pitman *et al.*, 2011; Lorenz *et al.*, 2014) within ACCESS. CABLE simulates the surface exchange of carbon, energy and water, representing the vegetation with a single layer, two-leaf (sunlit/shaded) canopy scheme (Wang & Leuning, 1998), and accounting for within-canopy turbulence (Raupach, 1994; Raupach *et al.*, 1997). The model simulates soil water and heat conduction across six discrete soil layers (ranging to 4.6 m depth), following the Richards equation. The standard model groups the vegetation into 11 PFTs, for global applications. CABLE has the capacity to simulate biogeochemistry (nitrogen and phosphorus) (Wang *et al.*, 2010) and vegetation demography model (Haverd *et al.*, 2014), but neither was enabled for these simulations as we prescribe the leaf area index (LAI), please refer to the following paragraphs.

The model source code can be accessed freely after registration at <https://trac.nci.org.au/trac/cable>. In this paper we used CABLE revision 8740.

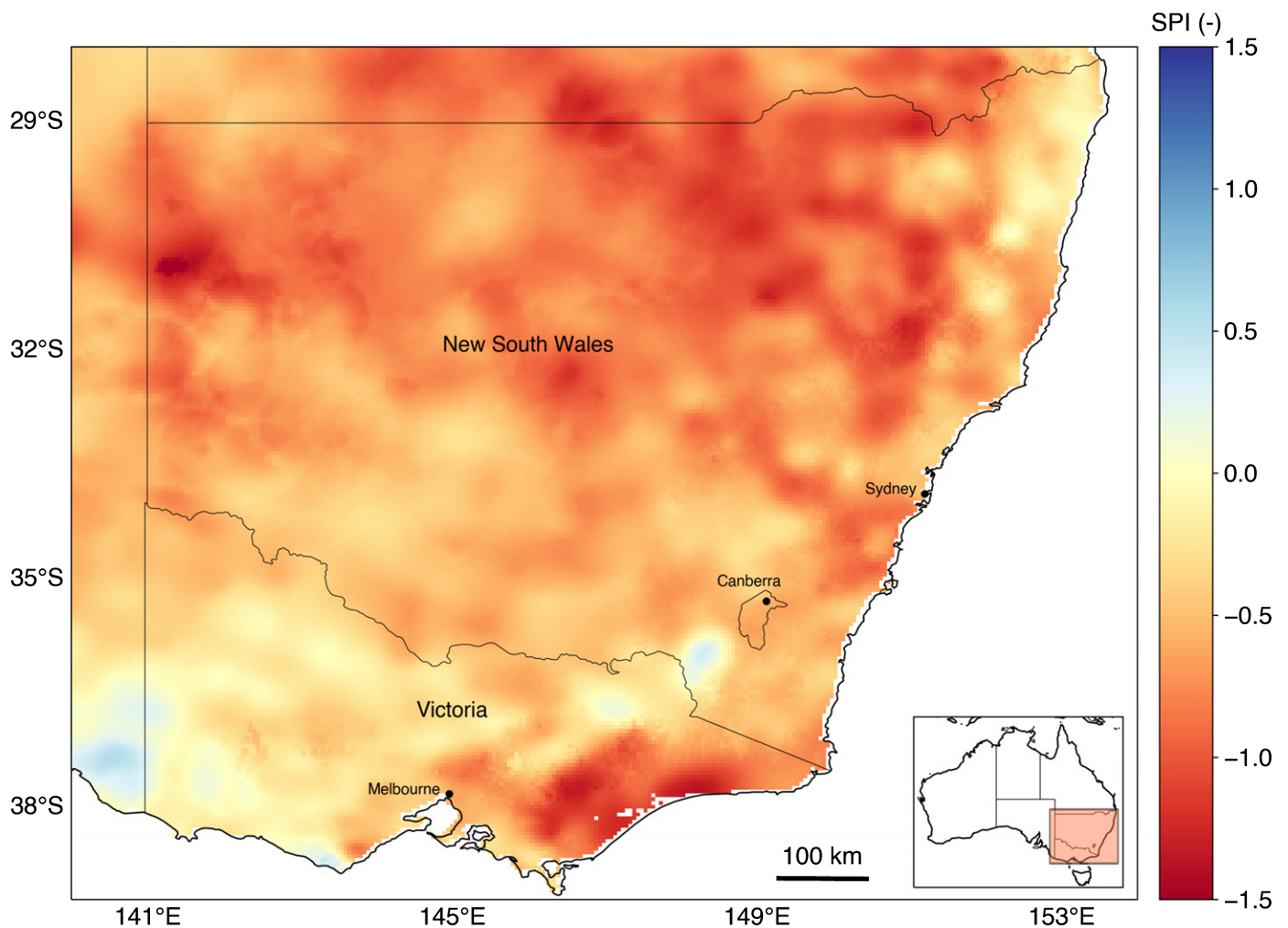


Fig. 1 Map of the mean Standardised Precipitation Index (SPI) anomaly during the drought (2017–2019). Anomalies were calculated relative to the historical baseline period of 1911–2016. Note we do not include data from after September 2019 onwards due to the confounding impact of fires across South-Eastern Australia.

Plant hydraulics implementation

Following Sabot *et al.* (2020), we introduced a simplified version of the profit maximisation scheme (Sperry *et al.*, 2017) into CABLE to replace the default gas exchange scheme and associated empirical representation of drought stress based on volumetric soil moisture content. Sperry *et al.* (2017) hypothesised that plants regulate their leaf water potential (Ψ_{leaf} ; MPa) on an instantaneous basis by weighing a marginal carbon gain (CG) against a hydraulic cost (HC) associated with transpiration, maximising profit as:

$$\text{Profit}_{\text{max}} = \max(\text{CG}(\Psi_{\text{leaf}}) - \text{HC}(\Psi_{\text{leaf}})) \in [0, 1] \quad \text{Eqn 1}$$

The normalised CG is given by:

$$\text{CG}(\Psi_{\text{leaf}}) = \frac{A(\Psi_{\text{leaf}})}{A_{\text{max}}} \in [0, 1] \quad \text{Eqn 2}$$

where A ($\text{mol m}^{-2} \text{s}^{-1}$) is the photosynthetic uptake, expressed as a function of each possible Ψ_{leaf} between the point of no transpiration (E) ($\Psi_{\text{leaf, predawn}} \approx \Psi_{\text{soil}}$, the soil water potential; MPa) and $E = E_{\text{crit}}$, the point of hydraulic failure. A_{max} ($\mu\text{mol m}^{-2} \text{s}^{-1}$) is the maximum photosynthetic rate over the range of possible Ψ_{leaf} .

To reduce the computational cost of introducing an optimisation scheme into a LSM, we directly link $A(\Psi_{\text{leaf}})$ to A expressed as a function of each possible leaf intercellular CO_2 concentration (C_i , $\{\text{mol mol}^{-1}\}$, $A(C_i)$, via the Farquhar model (Farquhar *et al.*, 1980) and Fick's law of diffusion applied to the supply of CO_2 through stomata. Therefore, instead of co-optimising C_i and stomatal conductance for every possible Ψ_{leaf} (as in Sperry *et al.*, 2017), we solve A across a sequence ($n = 1000$) of potential C_i , between the CO_2 compensation point in the absence of mitochondrial respiration (Γ^* , $\{\text{mol m}^{-2} \text{s}^{-1}\}$) and C_s . Each A is associated with a stomatal conductance rate to CO_2 (g_{sc} , $\text{mol m}^{-2} \text{s}^{-1}$) to represent the CO_2 flux from the leaf surface (C_s , $\{\text{mol mol}^{-1}\}$) to the leaf intercellular airspace (C_i , $\{\text{mol mol}^{-1}\}$). This in turn, defines the leaf transpiration rate (E_{leaf} , $\text{mmol m}^{-2} \text{s}^{-1}$) and then Ψ_{leaf} (please refer to Eqn 3 below), assuming that the water vapour exchange is proportional to stomatal conductance. This approach trades off a negligible degree of accuracy in the optimal solution as jumps in C_i were roughly the equivalent of $c. 0.35 \{\text{mol mol}^{-1}\}$, but significantly improves the computational efficiency which is necessary for LSMs.

The gas exchange calculations are solved iteratively within CABLE's loop that simulates the leaf temperature that closes the energy balance for the leaf (Wang & Leuning, 1998). Finally, Ψ_{leaf} is approximated by re-arranging the steady-state formulation:

$$\Psi_{\text{leaf}} = \Psi_{\text{soil, w}} - \frac{E_{\text{leaf}}}{k_{\Psi_{\text{leaf}}}} \quad \text{Eqn 3}$$

where $\Psi_{\text{soil, w}}$ is the weighted average of the soil water potential (MPa) and $k_{\Psi_{\text{leaf}}}$ is the soil-to-canopy conductance ($\text{mmol m}^{-2} \text{leaf s}^{-1} \text{MPa}^{-1}$), that is k_{max} evaluated at Ψ_{leaf} .

To reduce parameterisation, we do not solve separate xylem and leaf water potentials (as done in De Kauwe *et al.*, 2020). This water potential assumption and our incorporation of the leaf energy balance, are points of distinction from the original Sperry *et al.* (2017) model, with a final difference relating to how we obtain a representative Ψ_s , please refer to the following paragraph.

For each soil layer, the volumetric water content (θ , $\text{m}^3 \text{m}^{-3}$) is related to Ψ_s following Campbell (1974). To obtain a representative value of the root-zone Ψ_s , we weight the average Ψ_s for each of the six soil layers by the weighted soil-to-root resistance to water uptake of each layer (Williams *et al.*, 2001; De Kauwe *et al.*, 2015a). This approach weights Ψ_s to the upper soil layers when the root-zone is wet, but shifts towards the deeper soil layers as the soil dries and the soil hydraulic resistance of the layer increases (please refer to De Kauwe *et al.*, 2020).

The normalised HC (Eqn 1) is given by:

$$\text{HC}(\Psi_{\text{leaf}}) = \frac{k_{i\text{max}} - k_{\Psi_{\text{leaf}}}}{k_{i\text{max}} - k_{\text{crit}}} \quad \text{Eqn 4}$$

where $k_{i\text{max}}$ ($\text{mmol m}^{-2} \text{s}^{-1} \text{MPa}^{-1}$) is the instantaneous maximum plant hydraulic conductance attenuated by water stress (i.e. k_{max} evaluated at Ψ_{soil}), and k_{crit} ($\text{mmol m}^{-2} \text{s}^{-1} \text{MPa}^{-1}$) is the critical hydraulic conductance that characterises hydraulic failure, set to be 5% of k_{max} (Brodrribb & Cochard, 2009; Sabot *et al.*, 2020).

$k_{i\text{max}}$ and $k_{\Psi_{\text{leaf}}}$ are given by the cumulative Weibull distribution (Neufeld *et al.*, 1992):

$$k(\Psi) = k_{\text{max}} e^{-\left(\frac{\Psi}{b}\right)^c} \quad \text{Eqn 5}$$

where Ψ refers to the Ψ_s when calculating $k_{i\text{max}}$ and Ψ_{leaf} for $k_{\Psi_{\text{leaf}}}$. b (MPa) and c (unitless) are sensitivity and shape parameters of the plant hydraulic vulnerability curve. We assumed that cavitation can be fully recovered following rainfall and recharge of the root-zone, that is k can be fully recovered.

To infer the point of hydraulic failure, we track the percentage loss of hydraulic conductivity (PLC):

$$\text{PLC} = 100 \times \left(1 - \frac{k}{k_{\text{max}}}\right) \quad \text{Eqn 6}$$

A strong link has been shown between a threshold corresponding to an 88% loss of xylem hydraulic conductance (P_{88}) and drought mortality (Barigah *et al.*, 2013; Li *et al.*, 2015, 2018; Hammond *et al.*, 2019). Here, we do not directly equate P_{88} with mortality, but instead associate it with the vegetation approaching a point of hydraulic stress consistent with mortality, Ψ_{thresh} . This distinction is important because each grid cell ($c. 5 \text{ km}^2$) would contain some trees, not all of which would be dead. To properly associate Ψ_{thresh} to mortality would require stochastic approaches that are beyond the scope of the study. Please refer to Methods S1; Figs S2–S4 for a description of site validation.

Model simulations

Species distribution To obtain outputs at the species level we parameterised CABLE for 15 *Eucalyptus* species (please refer to below). Simulations were then run for each *Eucalyptus* species, assuming each species could grow across the domain of South-Eastern Australia. Model outputs were then filtered (postprocessed) by individual species distribution maps to relate outputs to individual *Eucalyptus* species. Species distribution maps were constructed from spatially referenced species occurrence records accessed from the Atlas of Living Australia for the period 1950–present (Andrew *et al.*, 2021). Species occurrence records were first quality controlled to remove erroneous spatial records and to standardise taxon names (Andrew *et al.*, 2021). Species distributions were constructed using Poisson point process models (PPMs) using regularised down-weighted Poisson regression (Renner *et al.*, 2015) based on 20 000 background points. PPMs were trained on mean annual temperature (°C), mean diurnal temperature range (°C), annual precipitation (mm), precipitation seasonality (coefficient of variation), annual mean radiation ($W m^{-2}$), aridity index, bedrock depth (m), soil bulk density (fine earth) in $kg m^{-3}$, clay mass fraction (%), silt mass fraction (%) and pH. These climate and soil factors (detailed in Renner *et al.*, 2015) were chosen as they reflect major abiotic factors shaping plants growth and nutrition in Australia.

Model parameterisation We used the hydraulic traits (Table 1) of 15 *Eucalyptus* species to parameterise the plant hydraulic vulnerability curve parameters (Eqn. 5). We used two hydraulic traits that describe the xylem pressure that induces a 12%, 50% or 88% loss of hydraulic conductivity due to embolism (i.e. P_{12} or P_{50} , or P_{88}). Lacking data to parameterise k_{max} by species, we assumed a fixed value of $1.5 mmol m^{-2} s^{-1} MPa^{-1}$ for each species. This value is in line with estimated values for European species with a mean annual precipitation *c.* 700–1100 $mm yr^{-1}$ (Sabot *et al.*, 2020), a range covering 11 of our 15 species. We carried out two experiments to examine the sensitivity to a smaller k_{max} value (please refer to below). We either used species data to parameterise the maximum carboxylation rate (V_{cmax}) or used an average across *Eucalyptus* species (Table 2).

Model forcing We ran offline simulations for South-Eastern Australia using gridded, 3-hourly meteorological forcing of precipitation, downward shortwave and longwave radiation, surface air temperature, surface specific humidity, surface wind speed, surface air pressure and CO_2 . We ran the model over the drought period from January 2017 to August 2019 (spin-up 2011–2016), at a resolution of 0.05° (*c.* 5 km^2). We excluded data from September 2019 onwards due to the potential contamination related to large-scale fires in South-Eastern Australia. The meteorological data are from the Bureau of Meteorology's AWAP dataset (Jones *et al.*, 2009) and the near-surface wind data of McVicar *et al.* (2008; McVicar, 2011).

CABLE was run with prescribed LAI based on a climatology (1999–2017) derived from the Copernicus LAI product (<http://land.copernicus.eu/global/>), regridded from a resolution of 0.01°

Table 2 Summary of photosynthetic trait parameter values.

Species	V_{cmax25} ($\mu mol m^{-2} s^{-1}$)	Reference
<i>Eucalyptus blakelyi</i>	86.88	*
<i>E. camaldulensis</i>	111.74	Zhou <i>et al.</i> (2016)
<i>E. crebra</i>	86.88	*
<i>E. dunnii</i>	86.88	*
<i>E. globulus</i>	85.55	C. Warren (2004); C. R. Warren (2004)
<i>E. grandis</i>	93.71	Leuning <i>et al.</i> (1991); Clearwater & Meinzer (2001); Grassi <i>et al.</i> (2002)
<i>E. largiflorens</i>	86.88	*
<i>E. macrorhyncha</i>	86.88	*
<i>E. melliodora</i>	86.88	*
<i>E. bliqua</i>	86.88	*
<i>E. populnea</i>	86.88	*
<i>E. saligna</i>	76.67	Ghannoum <i>et al.</i> (2010)
<i>E. sideroxydon</i>	100.37	Ghannoum <i>et al.</i> (2010)
<i>E. tereticornis</i>	86.88	*
<i>E. viminalis</i>	77.60	C. Warren (2004)

*The average species trait values from cited references in the Table 2 and Cernusak *et al.* (2011); Huang *et al.* (2008) and unpublished data from Drake *et al.* cited in Boer *et al.* (2016).

to 0.05° . By prescribing LAI we avoid the need for a long model spin-up, only requiring 5 yr to stabilise the soil temperature and root-zone soil moisture.

Soil properties (e.g. texture, soil hydraulic and thermal characteristics) for CABLE were based on the SoilGrids data (Hengl *et al.*, 2017). Data were degraded using local area averaging from 250 m to 0.05° for simulations. As is standard in CABLE, we assumed vertically uniform soil texture based on the weighted average of the 2 m SoilGrids data.

Experiments

We ran three sets of simulations:

- (1) A control simulation ('CTL'), representing the 2017–2019 drought in South-Eastern Australia.
- (2) A 20% reduction in the 2017–2019 precipitation to represent a future drier (please refer to below) drought ('rPPT').
- (3) To explore how a CO_2 -induced change in plant water-use efficiency (De Kauwe *et al.*, 2021) may delay the onset of drought conditions, we combined the rPPT experiment with a doubling of the $[CO_2]$ to *c.* 800 $\mu mol mol^{-1}$ (' $eCO_2 \times rPPT$ ').

Climate model projections of historic and future precipitation contain systematic biases for Australia (Alexander & Arblaster, 2017; Grose *et al.*, 2020). Continental mean annual precipitation estimates range from *c.* 200 to 1200 $mm yr^{-1}$, with observed-derived estimates *c.* 400 $mm yr^{-1}$ (L. Teckentrup *et al.*, unpublished). Options to correct precipitation include bias correction and the use of regional climate models to dynamically downscale and generate fine scale climate projections. A preliminary analysis of one corrected dataset (the NSW and ACT Regional Climate Model, NARCLiM project) highlighted unrealistic interannual variability in precipitation (e.g. annual precipitation varying between 250 and 2250 $mm yr^{-1}$). Given these

marked biases in the use of future climate precipitation forcing, we opted for a simpler, uniform reduction in the AWAP rainfall (i.e. rPPT). Our approach maintains a plausible future experiment but does not account for changes in the distribution of humidity and precipitation deficit. The rPPT experiment also allows us to probe the impact of the original drought, which extended to the end of 2020 but was affected by the 2019–2020 South-Eastern Australia fires (Nolan *et al.*, 2020).

Sensitivity experiment To understand how our model assumptions affected simulated drought risk, we carried out three sensitivity experiments at a single location near Armidale, New South Wales (−30.40°S, 151.60°E) during the 2017–2019 drought. This area was reported as having experienced notable foliage dieback during the drought (Nolan *et al.*, 2021). In each experiment, we plotted the change in stomatal conductance (g_{sw}) as a function of Ψ_{leaf} and examined the resulting impact on the relative loss of hydraulic conductance. We varied: (1) the critical leaf water potential indicative of maximum xylem hydraulic failure (k_{crit}); (2) the maximum hydraulic conductance in the soil–plant continuum (k_{max}); (3) the LAI by increasing it by 40% (eLAI); (4) and the $[CO_2]$, by doubling it, in combination with a 40% increase in LAI ($eCO_2 \times eLAI$). To further understand the sensitivity to halving k_{max} , we also repeated all of the main experiments across South-Eastern Australia (CTL, rPPT and $eCO_2 \times rPPT$) with the halved k_{max} value.

Data sets used

Satellite data To evaluate CABLE, we calculated anomaly maps (percent difference) using remote sensing estimates of vegetation optical depth (VOD; 2002–2016 baseline) and the normalised difference vegetation index (NDVI; 2001–2016 baseline). VOD describes the attenuation of microwave wavelengths through vegetation and is most sensitive to above-ground vegetation water content and changes in leaf/branch biomass (Dijk *et al.*, 2013). NDVI quantifies the photosynthetically active radiation that is absorbed by vegetation, and therefore reflects the foliar vegetation state. We used the land parameter data record (LPDR) v.3 VOD product (Du *et al.*, 2017), which uses retrievals from the Advanced Microwave Scanning Radiometer for EOS (AMSR-E) and the Advanced Microwave Scanning Radiometer 2 (AMSR2). For NDVI, we used the MOD13A2 (collection 006) product (<https://lpdaac.usgs.gov/products/mod13a2v006/>).

Analysis code

All analysis code is freely available from: https://github.com/mdekaue/SE_AUS_future_drought_risk_paper.git

Results

Minimum water potential

Fig. 2 summarises the impact of the drought expressed as the minimum water potential (Ψ_{min}) reached during the 2017–2019

for each species and for each of our three experiments (Figs S5–S7 show distribution maps). As Ψ_{min} represents the absolute minimum water potential during the drought, it characterises the dehydration tolerance of each species across its distribution. The box and whiskers show the variability of Ψ_{min} between experiments across a species' distribution, with the distance between a species' median and the water potential inducing a 50% loss in hydraulic function (P_{50}), indicative of the degree of overall stress (please refer to also Fig. 3). The severity of the drought is underlined by several species experiencing levels of stress that pushed the (median of the distribution) Ψ_{min} close to (*E. populnea*, *E. melliodora*, *E. blakeyi*, *E. tereticornis* and *E. saligna*), or beyond (*E. sideroxylon*, *E. crebra* and *E. grandis*), P_{50} . The simulated Ψ_{min} was not strictly related to background dryness (mean annual precipitation), with both mesic and xeric species impacted by the drought (i.e. more negative Ψ_{min}).

Our experiment extending the impact of the drought (rPPT; a proxy for the impact of the real drought that extended to the end of 2020, please refer to the **Materials and Methods** section) had a greater impact on species with a lower embolism resistance (higher P_{50} ; for example *E. macrorhyncha* and *E. viminalis*) and species with a southern ('wetter') distribution (Fig. 2). Overall, the impact of the reduced rainfall was a further reduction in Ψ_{min} relative to CTL (median: −16%, range: −31.7% to −1.5%), although for many species the difference between the CTL and rPPT was limited (e.g. *E. largiflorens*, *E. populnea*, *E. crebra*), implying that some species were already extremely droughted across their distributions. By contrast, doubling the $[CO_2]$ (rPPT \times eCO_2) had a profound impact on Ψ_{min} , increasing the overall median Ψ_{min} by 32% (range: 7–59%) relative to the rPPT experiment. For most species, doubling $[CO_2]$ led to a much less negative median Ψ_{min} (e.g. *E. blakeyi*, *E. ideroxylon*, *E. melliodora*, *E. macrorhyncha*), with a few notable exceptions (*E. populnea*, *E. crebra* and *E. largiflorens*).

To emphasise the drought impact on each species, Fig. 3 shows the proportion of each species' distribution for which the mean monthly Ψ_{leaf} was below P_{50} . For the CTL experiment, most species ($n = 9$) experienced lower Ψ_{leaf} than P_{50} for at least 25% of their range, with *E. sideroxylon*, *E. blakeyi*, *E. crebra* and *E. tereticornis* over 50% of their range. The rPPT experiment had the greatest relative (CTL vs rPPT) impact on *E. obliqua* and *E. globulus*, more than doubling the proportion of the range below P_{50} . By contrast, doubling $[CO_2]$ had the least ameliorating impact of drought on *E. crebra* and most on *E. dunnii*.

Maximum loss of hydraulic conductivity

Fig. 4 shows the maximum loss of hydraulic conductivity (PLC), for each species across its distribution for the CTL experiment (Figs S8, S9 show the rPPT and $eCO_2 \times rPPT$ maps, respectively). Although the overall loss in conductivity was significant (40%), the impact of drought varied within a species distribution (greatest in the North-East) and even between species with similar distributions (cf. *E. blakeyi*, *E. macrorhyncha* and *E. viminalis*).

Drought hotspots (PLC = 88%) where drought-induced hydraulic failure could be anticipated were evident for

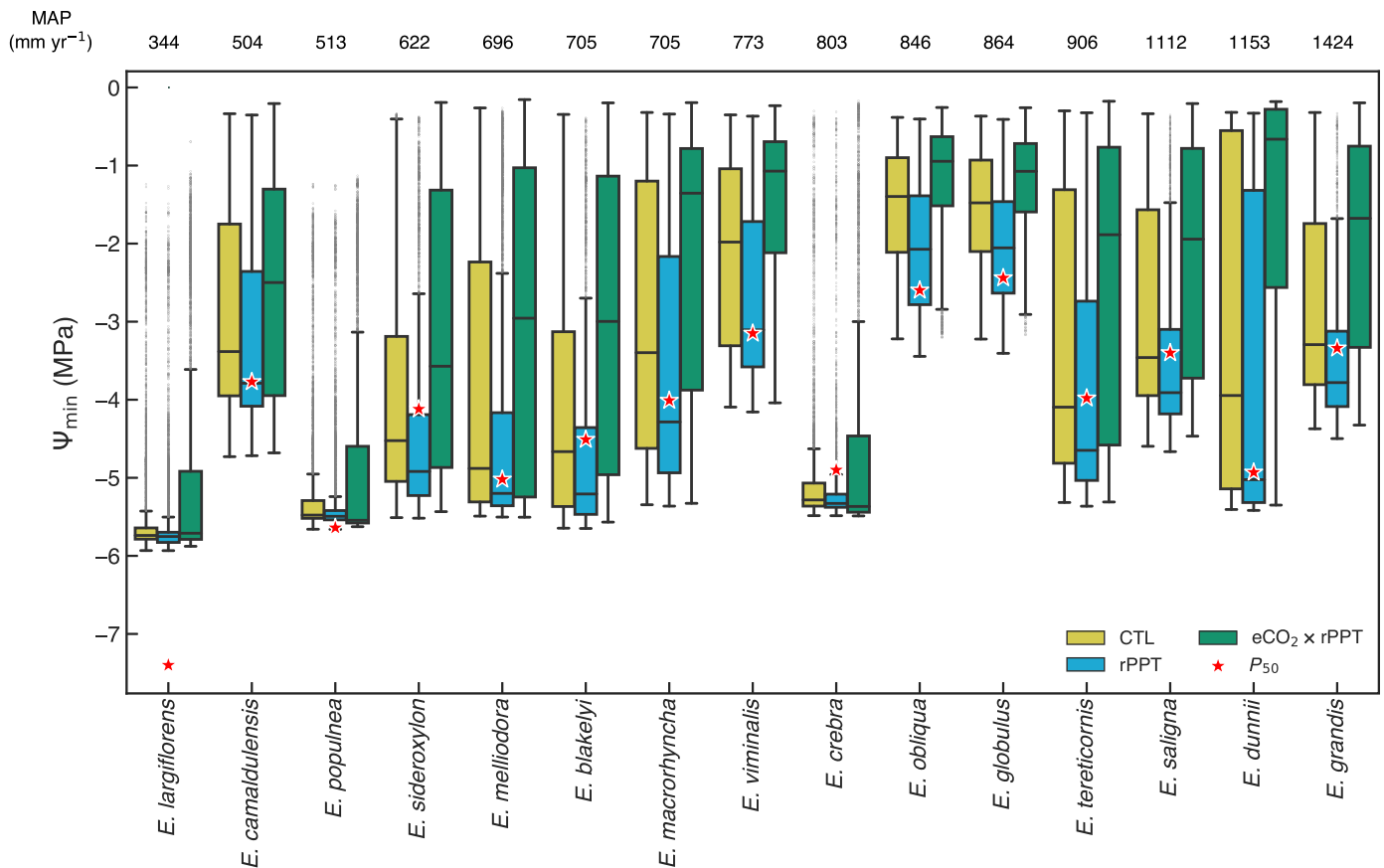


Fig. 2 Box and whisker plot (line, median; box, interquartile range) showing the range of simulated minimum leaf water potential (Ψ_{\min}) across a species' distribution for each of the three experiments: 2017–2019 drought (CTL), 20% reduction in rainfall during the drought (rPPT) and 20% reduction in rainfall during the drought in combination with a doubling of atmospheric carbon dioxide, CO_2 ($\text{eCO}_2 \times \text{rPPT}$). The *Eucalyptus* species are ordered from the driest to the wettest, with each species' mean annual precipitation (MAP) across their range, above each set of box plots. The red stars show each species' P_{50} , the xylem pressure inducing 50% loss of hydraulic conductivity due to embolism. Whiskers extend to 1.5 times the interquartile range, with dots outside of the whiskers showing outliers.

E. viminalis, *E. obliqua*, *E. globulus*, *E. saligna* and *E. grandis*. By contrast, several species appeared resilient to the impacts of the drought (*E. largiflorens*, *E. populnea*, *E. melliodora* and *E. crebra*), simulating moderate values of PLC (< 40%). Similarly, several species (*E. melliodora*, *E. crebra*, *E. blakelyi*) had overlapping ranges with hotspots for other species, yet were seemingly resilient due to their more tolerant hydraulic traits. The impact was overall greatest for *E. camaldulensis*, which, despite growing in more arid locations (mean annual precipitation [MAP] across the range = 504 mm yr⁻¹), is relatively more sensitive to drought stress than other species (less negative P_{50} ; Fig. 2) in our model simulations. *E. camaldulensis* ('river red gum') typically grows along rivers, creeks and waterways and this proximity to a water source is not considered by CABLE, therefore leading to a likely overestimation of the impact of drought.

Model sensitivities

We identified three key assumptions to which our model results were sensitive. First, given how low some of our simulated species Ψ_{\min} values were, we asked whether the optimisation model has sufficient stomatal control as turgor is lost. Examining midday

g_{sw} as a function of midday Ψ_{leaf} (Fig. 5a) does suggest that the optimisation scheme does not sufficiently regulate stomata. We can see a few higher (perhaps unrealistic) g_{sw} values at more negative midday Ψ_{leaf} values (< -3 MPa), implying the optimisation scheme obtained marginal 'profit' by keeping stomata open, despite strong water-limiting conditions. Increasing the k_{crit} value increases the plant's stomatal control and therefore decreases the PLC (Fig. 5d).

Second, we did not have data to parameterise k_{max} , therefore we used the same value for every species. Fig. 5b clearly shows that halving this value significantly reduces evaporative losses and is the difference between CABLE simulating zero PLC and near hydraulic failure (Fig. 5e).

Fig. 2 highlighted the sensitivity Ψ_{\min} values to a doubling of [CO_2]; however, as LAI was prescribed in our simulation, we have not accounted for the potential effect of [CO_2]-induced increases in LAI (Rifai *et al.*, 2021). Fig 5c,f shows that a 40% increase in LAI would lead to hydraulic failure (PLC = 88%) relative to the control, as evaporative losses were greater. However, our combined simulation of increased LAI (which ignores the potential for drought-induced defoliation) and a doubling of [CO_2] ($\text{eCO}_2 \times \text{eLAI}$; Figs 2, S7, S9) suggested that the CO_2

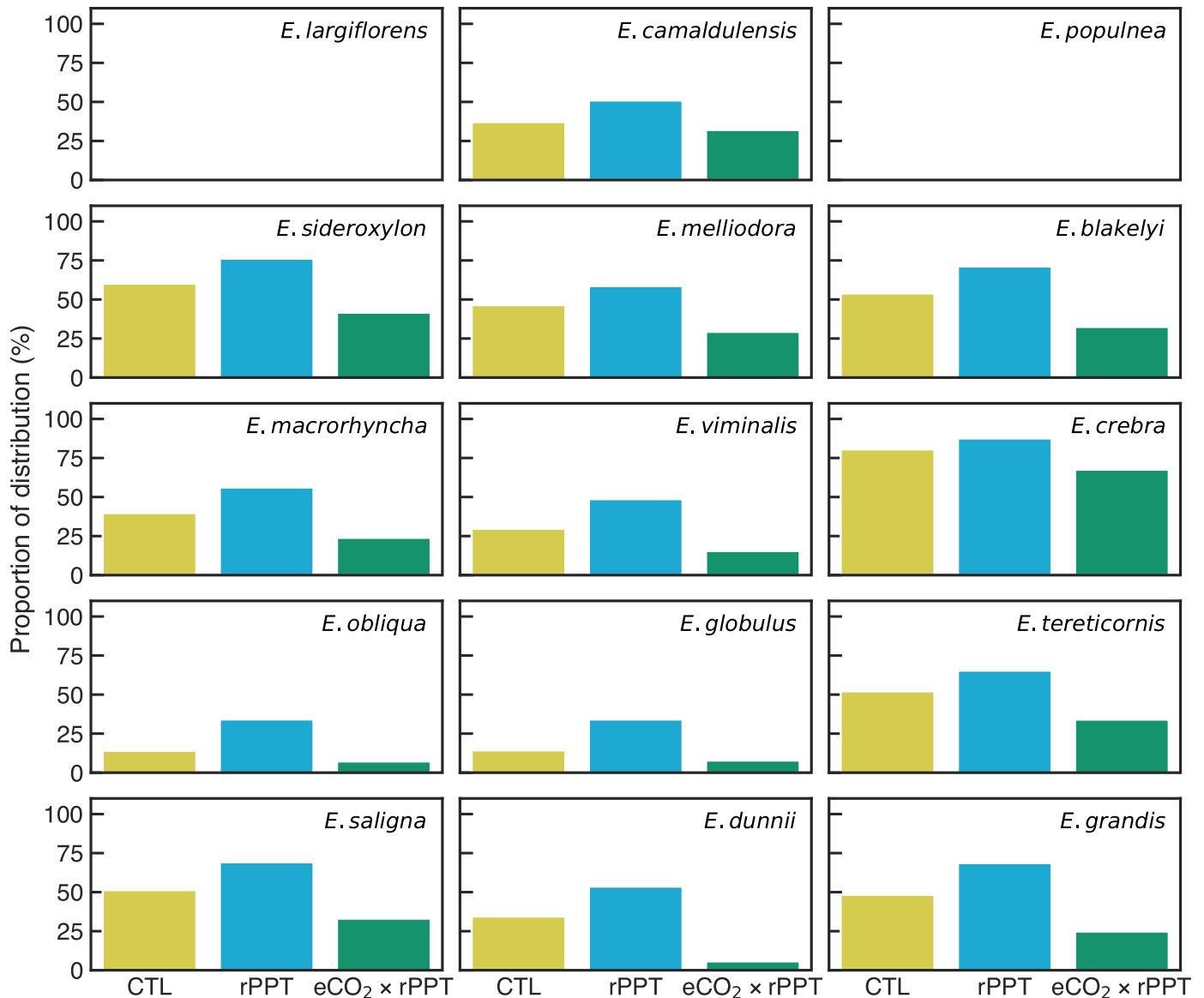


Fig. 3 The proportion of each species' distribution where the simulated mean monthly leaf water potential (Ψ_{min}) dropped below (more negative) than each species' P_{50} , the xylem pressure inducing 50% loss of hydraulic conductivity due to embolism. Bars indicate each of the three experiments: 2017–2019 drought (CTL), 20% reduction in rainfall during the drought (rPPT) and 20% reduction in rainfall during the drought in combination with a doubling of atmospheric carbon dioxide, CO₂ (eCO₂ × rPPT). The species are ordered from the driest (*Eucalyptus largiflorens*) to the wettest (*E. grandis*), based on mean annual precipitation and matching the order in Fig. 2.

effect on plant water-use efficiency cancels out the effect of increased LAI, such that there was no increased risk of hydraulic failure.

Focussing further on the sensitivity of k_{max} , Fig. 6 shows the effect of halving k_{max} on the simulated PLC at the landscape scale (Figs S10, S11 show the rPPT and eCO₂ × rPPT maps, respectively). Comparing Figs 4 and 6, we can see that for all species, the apparent mortality risk is greatly reduced. Despite this, we still see a key hotspot (*c.* 32°S and *c.* 150°E) where PLC exceeds 60% for multiple species (*E. sideroxylon*, *E. blakelyi*, *E. macrorhyncha*, *E. viminalis*, *E. tereticornis*, *E. saligna* and *E. grandis*) and other more widespread reductions in PLC > 30% (*E. populnea*, *E. melliodora* and *E. crebra*), despite the reduction in k_{max} .

Validation

Assessing the accuracy of landscape-scale, species-level mortality risk predictions is challenging because: (1) other nontree species (e.g. crops) contribute to the signal; (2) remotely sensed estimates do not directly detect mortality; and (3) knowledge of both species occurrence and species density is required to scale up model simulations. Noting these challenges, we opted to equally weight PLC by species occurrence in a pixel. Fig. 7 therefore shows a crude comparison of PLC simulated by CABLE to remotely sensed anomaly maps of drought impact. CABLE's simulation of PLC weakly correlated with VOD ($r = -0.1$; Fig. 7a) and NDVI ($r = -0.21$; Fig. 7b). CABLE overstates the extent of the worst-hit regions (north of 35°S and between 149°E to

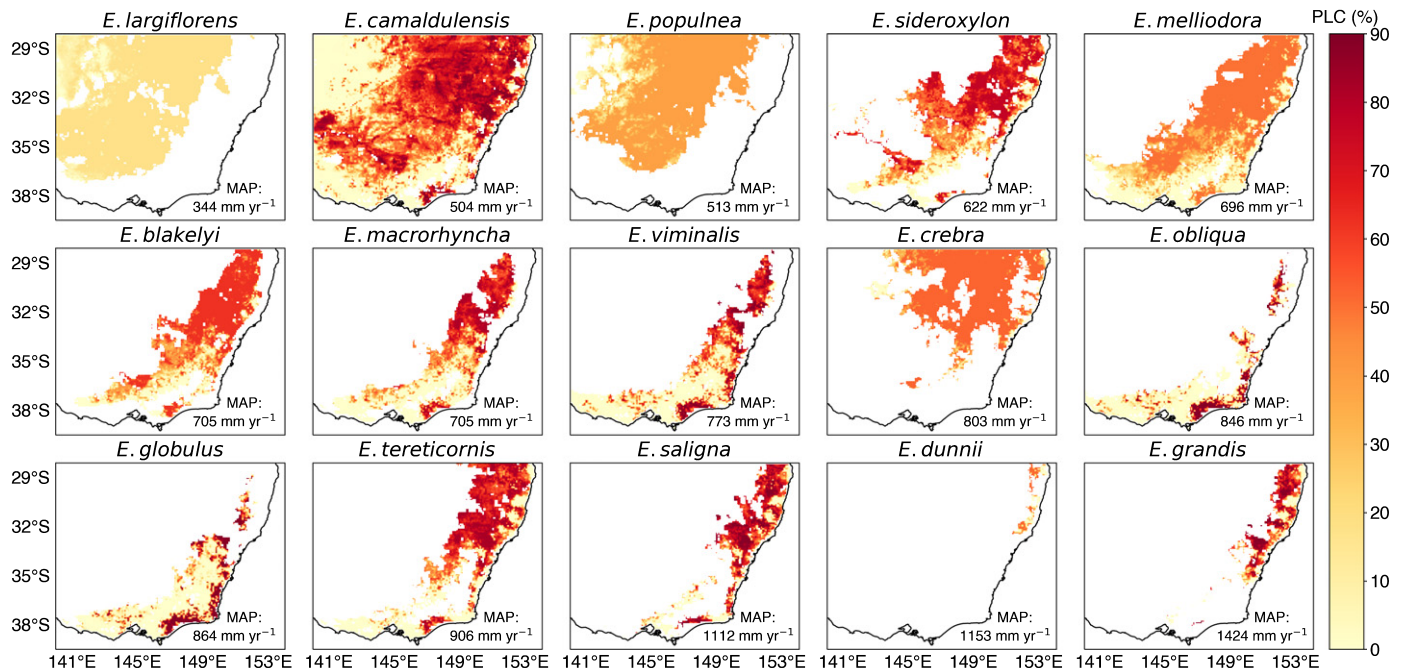


Fig. 4 Maps showing the maximum percentage loss of hydraulic conductivity (%) simulated by Community Atmosphere Biosphere Land Exchange (CABLE) during the drought (2017–2019), control (CTL) experiment. The *Eucalyptus* species are ordered from the driest to the wettest, with each species' mean annual precipitation (MAP) across their range, indicated in each panel. Note we do not include data from after September 2019 due to the confounding impact of fires across South-Eastern Australia.

151°E), as this hotspot is not evident in the VOD map, and to a lesser extent in the NDVI map. However, there is clear agreement between the region with the greatest anomaly in the satellite maps (north of 32°S and between 147°E to 149°E) and the area where PLC values exceed 50%. CABLE also highlights a hotspot in East Gippsland, in southern Victoria that is present in the SPI map (Fig. 1).

Discussion

Identifying how drought risk varies across species ranges

To improve predictions of the impact of future droughts and heatwaves on ecosystems, we need to develop the capacity to accurately forecast near-term ecological responses (Dietze *et al.*, 2018). However, this cannot be achieved with existing modelling frameworks (e.g. CMIP6), as they currently lack key relevant physiological mechanisms and also do not simulate responses at the species level, hindering the potential to inform land management decisions. Our results represent an important advance in the capacity to forecast tree species resilience to drought across South-Eastern Australia, providing a new evidence base for decision-making around the long-term resilience of a broad range of species used in restoration plantings.

CABLE identified several drought hotspots across the ranges of *E. viminalis*, *E. obliqua*, *E. globulus*, *E. saligna* and *E. grandis* (Fig. 4). The rPPT experiment most affected *E. obliqua* and *E. globulus* (Fig. 3), more than doubling the proportion of their range below P_{50} , whilst for other species, the impact was *c.* 14

percentage points (min = 0; max = 19). The rPPT experiment points to the likely importance of the continued stress imposed by the drought during 2019–2020 bushfires. Our simulations suggested considerable hydraulic failure risk for *E. camaldulensis*, although whether this risk emerged in reality relates to subsurface water availability and extraction in rivers and creeks that our model does not capture. CABLE highlighted resilience to drought in species that are found predominantly in semiarid areas such as *E. largiflorens* and *E. populnea*. CABLE pinpointed the role of hydraulic traits in conferring resilience for species with overlapping distributions (cf. *E. blakelyi* to *E. saligna*) subject to marked precipitation deficits.

Although we did identify uncertainty to our assumed k_{\max} value (Figs 5, 6), plant hydraulic conductances (per unit leaf area) (De Kauwe *et al.*, 2020) for Australian species are consistent with our assumed value (even for arid species), implying our sensitivity experiment is an uncommon scenario. Furthermore, the improved simulations of carbon and water fluxes during periods of water stress at Australian flux sites (Figs S2–S4) and the qualitative spatial agreement between our weighted simulations and satellite derived VOD (cf. Figs 4, 5) provide confidence in the robustness of our model simulations to our assumed k_{\max} .

Notably, our results differ from an application of CABLE with a different plant hydraulics scheme (De Kauwe *et al.*, 2020). First De Kauwe *et al.* (2020) identified greater risk of hydraulic failure in the most arid regions (e.g. north of 32°S and west of 145°E) when compared with this study. In both studies, the vegetation type ('semiarid woodland') and species covering most of that region (*E. largiflorens*) had resilient hydraulic traits ($P_{50} < -7$

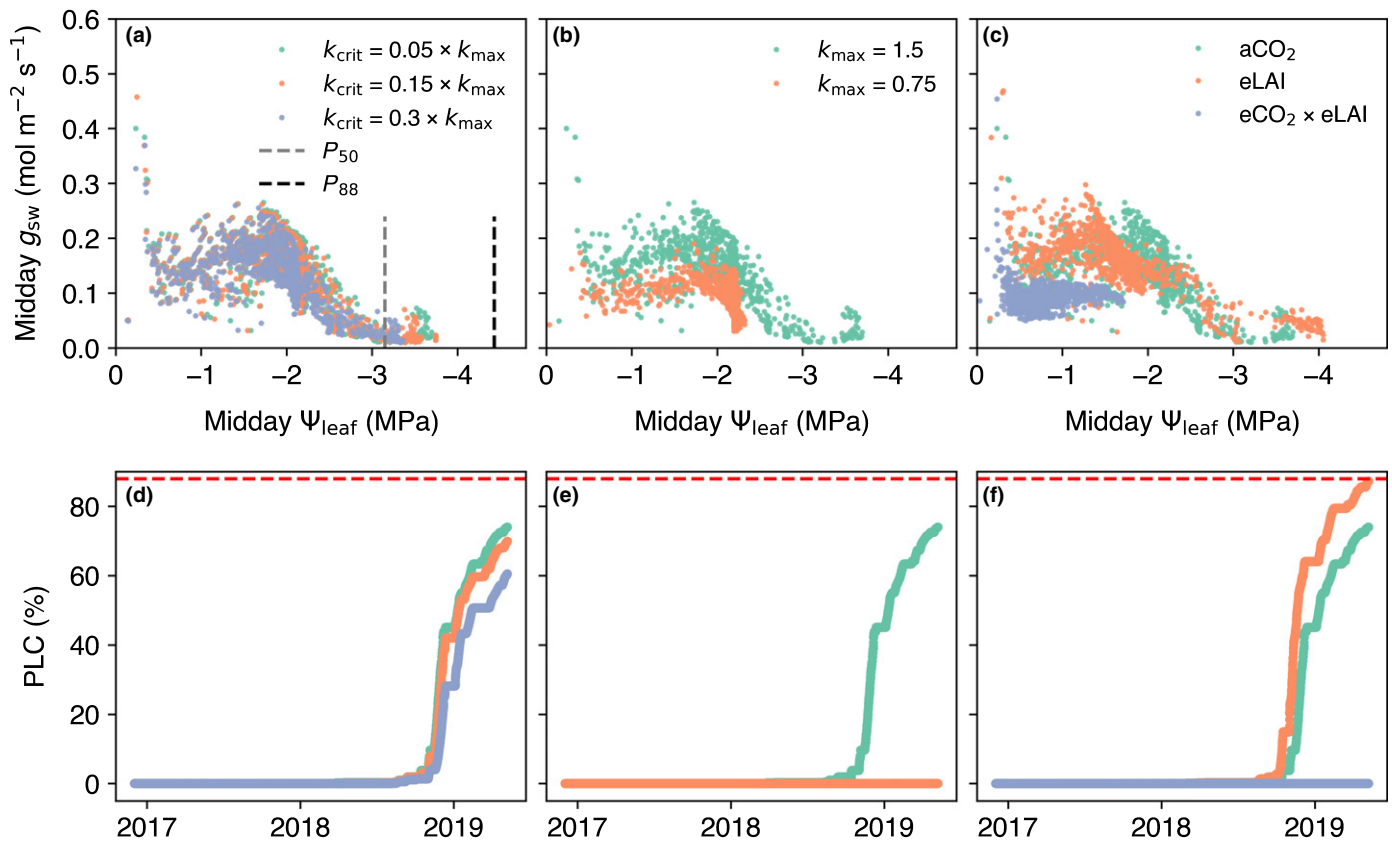


Fig. 5 Community Atmosphere Biosphere Land Exchange (CABLE)'s sensitivity to the assumed: (i) critical leaf water potential indicative of maximum xylem hydraulic failure (k_{crit} ; $\text{mmol m}^{-2} \text{s}^{-1} \text{MPa}^{-1}$); (ii) the maximum hydraulic conductance in the soil–plant continuum (k_{max} ; $\text{mmol m}^{-2} \text{s}^{-1} \text{MPa}^{-1}$); and a 40% increase in leaf area index (eLAI) and a doubling of the CO_2 concentration from ambient (a CO_2) and a 40% increase in leaf area index (e $\text{CO}_2 \times \text{eLAI}$). Panels (a–c) show the midday stomatal conductance (g_{sw}) as a function of midday leaf water potential (Ψ_{leaf}). Panels (d–f) show the corresponding impact of different assumed values in panels (a–c), respectively, on the simulated percentage loss of hydraulic conductivity (PLC). The dotted horizontal red line indicates the water potential inducing a critical loss in function (i.e. an 88% loss of hydraulic conductivity). All simulations are from a location near Armidale, New South Wales (30.4°S, 151.6°E).

MPa). One point of difference was the higher assumed plant hydraulic conductance (based on experimental data), which may have exacerbated the depletion of soil water in the earlier study. A second difference relates to the role of g_{min} (cuticular conductance) that was used in the ‘second’ drought phase in that version of the model (Choat *et al.*, 2018). This implies that in the De Kauwe *et al.* (2020) study, complete stomatal closure was simulated due to high vapour pressure deficit (and a continued loss of water via g_{min} after stomatal closure, please refer to the following paragraphs), which was not the case with the profit maximisation approach in this study. Capturing the correct stomatal sensitivity as vapour pressure deficit increases is emerging as a key knowledge gap across models, particularly at high vapour pressure deficit (Yang *et al.*, 2019). Sabot *et al.* (2022) demonstrated wide variability in the sensitivity of stomatal conductance to vapour pressure deficit across the latest generation of optimal stomatal models (Wolf *et al.*, 2016; Sperry *et al.*, 2017; Dewar *et al.*, 2018; Eller *et al.*, 2018). However, as the sensitivity to vapour pressure deficit emerges from the parameterisation of the hydraulic vulnerability curve and the optimisation target, this uncertainty cannot be easily constrained with observations.

Stomatal control

We hypothesised that the negative drop in Ψ_{min} (i.e. close to or below the P_{50} ; Fig. 2) may relate to degree of stomatal control in the profit maximisation model (Fig. 5a,d). In earlier work, Sabot *et al.* (2020) identified the importance of the k_{crit} parameter for determining the overall stomatal control of the profit maximisation model. This parameter is uncertain, varying by species in relation to the point of complete hydraulic failure, which makes it hard to determine *a priori*. Our results showed potentially unrealistic stomatal control at very negative Ψ_{leaf} values, where the model increased g_{sw} to achieve marginal CGs (Fig. 6a). By contrast, for *Eucalyptus* species, observations point to a strong relationship between the xylem water potential at 90% stomatal closure and the xylem water potential at the inception of xylem cavitation (P_{12}) (Li *et al.*, 2018), implying strong stomatal control. Whilst increasing k_{crit} would mute this behaviour, it would not completely stop it, so this remains an area for further analysis.

Alternatively, one could hypothesise that the apparent lack of stomatal control reflects the fact that we are not also attenuating

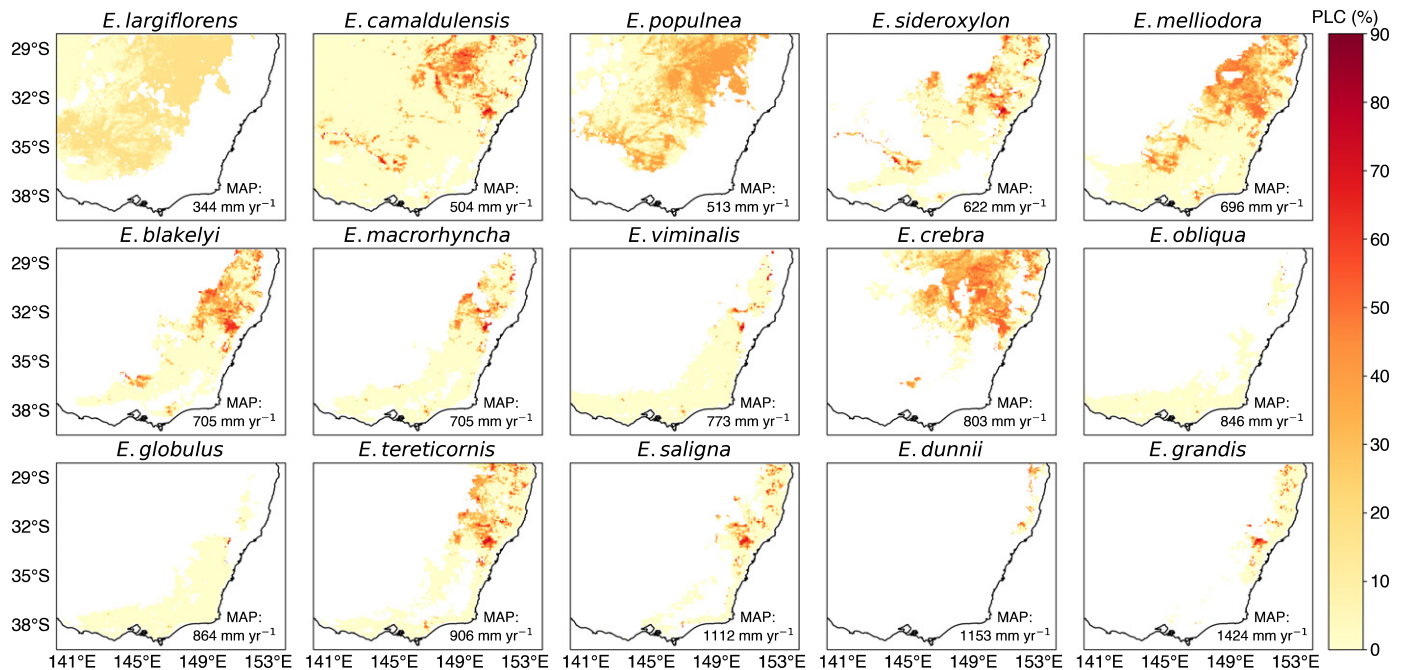


Fig. 6 Maps showing the maximum percentage loss of hydraulic conductivity (%) simulated by Community Atmosphere Biosphere Land Exchange (CABLE) when the maximum hydraulic conductance in the soil–plant continuum (k_{\max}) is halved for the 2017–2019 drought (control (CTL) experiment). The *Eucalyptus* species are ordered from the driest to the wettest, with each species' mean annual precipitation (MAP) across their range, indicated in each panel. Note we do not include data from after September 2019 due to the confounding impact of fires across South-Eastern Australia.

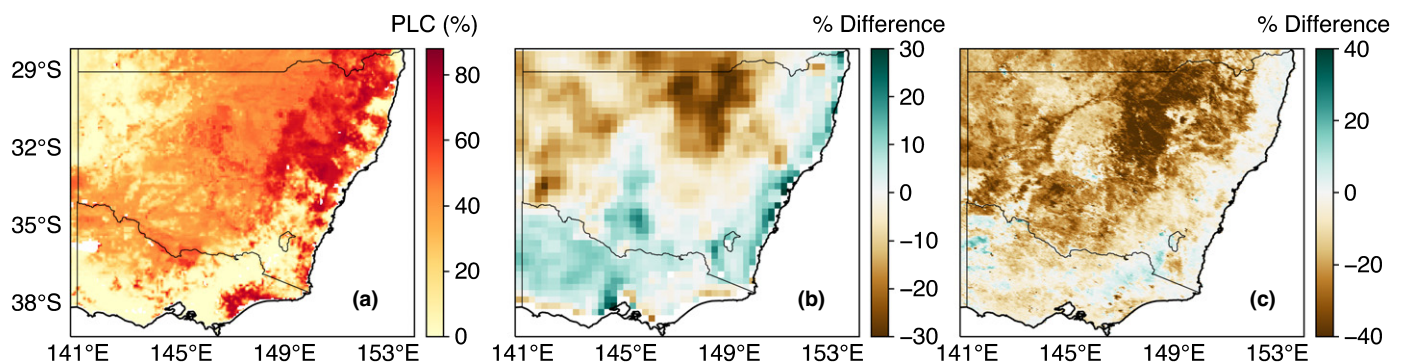


Fig. 7 Maps showing (a) the species weighted (by species occurrence in a pixel) maximum loss of hydraulic conductivity simulated by Community Atmosphere Biosphere Land Exchange (CABLE) during the drought (2017–2019). (b) The percentage difference between the mean vegetation optical depth (VOD) during the drought relative to 2002–2016. (c) The percentage difference between the mean normalised difference vegetation index (NDVI) during the drought relative to 2001–2016. Note for all panels, we do not include data from after September 2019 onwards due to the confounding impact of fires across South-Eastern Australia.

V_{cmax} through 'non-stomatal limitations' (Zhou *et al.*, 2013) as soil water becomes limiting. In our simulations, a greater direct constraint on photosynthesis would reduce the marginal benefit delivered by opening stomata at very negative Ψ_{leaf} values. Previous studies using empirical, rather than optimisation models, have demonstrated the need to capture both stomatal and non-stomatal limitations during drought (Keenan *et al.*, 2010; Zhou *et al.*, 2013; De Kauwe *et al.*, 2015a).

Similarly, eucalypt access to groundwater (Christina *et al.*, 2017; Zolfaghar *et al.*, 2017) reflects an important water source that may reduce simulated vulnerability during droughts. Recently, Mu *et al.* (2021) showed that incorporating a

groundwater scheme into CABLE (without plant hydraulics) increased transpiration by *c.* 100 mm yr⁻¹ during the 2017–2019 drought, predominantly by reducing vertical drainage. Future model developments that link improvements in plant hydraulics to improvements in subsurface hydrology, including the role of deeper root water access (via tap roots, but please refer to Pivovarov *et al.*, 2021), are needed.

An outstanding question for the new generation of stomatal optimisation models (Wolf *et al.*, 2016; Sperry *et al.*, 2017; Dewar *et al.*, 2018; Eller *et al.*, 2018) is whether they are capturing the correct degree of stomatal control, or instead if this reflects other process gaps (e.g. non-stomatal limitations,

groundwater, etc.). Specifically, one could ask whether an apparent lack of sufficient control should be expected given these models are linking fast processes (i.e. stomatal opening/closure) to slow processes (i.e. investment in architecture to avoid hydraulic failure), via the cost function (Wolf *et al.*, 2016; Sperry *et al.*, 2017). More data is needed to determine whether avoiding embolism (represented via the vulnerability curve) is the primary control on stomatal closure, or whether other primary, active controls need to be represented (e.g. abscisic acid accumulation Farquhar & Sharkey, 1982). To emphasise this point, Martin-StPaul *et al.* (2017) reported a very small range in the point of stomatal closure relative to a range of P_{50} values across species, implying additional stomatal regulation may be required.

The role of [CO₂] in ameliorating plant drought stress

Reduced stomatal conductance in response to rising [CO₂] and therefore, increasing soil water content ('water savings') has long been hypothesised as a mechanism by which plants may ameliorate the impact of drought (Medlyn *et al.*, 2001); however, the evidence is equivocal (De Kauwe *et al.*, 2021). For all but three of our species (*E. largiflorens*, *E. populnea* and *E. crebra*), doubling [CO₂] offset (via increased water-use efficiency) a considerable proportion of the negative effect of a further reduction in rainfall across South-Eastern Australia (rPPT). The apparent lack of sensitivity of these three species (*E. largiflorens*, *E. populnea* and *E. crebra*) in fact reflects the duration of moisture stress across their distribution. That is, where the duration of water stress conditions was prolonged (and severe), the capacity of increased plant water-use efficiency to ameliorate drought stress was negligible. This result can be seen most clearly either by contrasting distribution medians in Fig. 2, or by comparing the lack of change in PLC between the rPPT (Fig. S8) and eCO₂ × rPPT (Fig. S9) experiments. By contrast, for the other species, it is striking that the increase in Ψ_{\min} was typically found in the southern (typically wetter) parts of distribution ranges (cf. Figs S6, S7), implying a specific role of CO₂ in ameliorating stress.

Our results are consistent with modelling approaches that have considered responses under future climate. Sperry *et al.* (2019) used a more complicated implementation of the profit maximisation approach applied across continental USA and found a strong role for elevated [CO₂] in offsetting drought effects. They also showed that future temperature rises could negate these benefits, which we did not test in our future simulations (although our CTL simulation did include high temperatures associated with the drought, particularly in January 2019). Cochard *et al.* (2021) simulated lethal embolism rates for a single oak tree species under a future Representative Concentration Pathways scenario (very high emissions, RCP8.5), attributing the driver to increasing vapour pressure deficit (please refer to below). This strong link to vapour pressure deficit is likely to reflect the assumed temperature sensitivity of cuticular conductance in their model, although support for a link between cuticular conductance and temperature is an important issue to resolve (please refer to Slot *et al.*, 2021). Anderegg *et al.* (2015) derived an empirical threshold between observed mortality in *P. tremuloides* and climatic water deficit to

determine the likely future timescale of mortality based on coupled climate models. However, this type of approach does not allow for plant responses to [CO₂] to affect the time point at which this threshold is reached, which may overstate risk. Future work is still required to determine whether models are capturing the correct sensitivity to [CO₂] when projecting the role of drought stress. This remains one area for which it is particularly challenging to scale from manipulation experiments to models, due to the numerous real-world interactions (please refer to De Kauwe *et al.*, 2021).

How to parameterise k_{\max}

One important simplification we made in our simulations was to assume that species had the same k_{\max} : this is unrealistic given the breadth of arid conditions occupied across the species distributions. Accurate parameterisation of this key parameter at the ecosystem scale is important, but unfortunately this is not a trait that is routinely reported. Theoretically, where sap flow or eddy covariance data capture individual species evaporative fluxes, the maximum conductance of a plant could be determined. Unfortunately, few eddy covariance sites cover the domain of interest in this study and/or have species that overlap with those for which hydraulic traits have been characterised (Wombat State Forest being the exception – *E. obliqua*).

Alternatively, Sperry *et al.* (2017) hypothesised that the optimal k_{\max} should be associated with V_{\max} , which is an attractive solution as a relationship between maximum water conductance and maximum CG makes theoretical sense. Nevertheless, it remains unclear exactly how k_{\max} could be directly obtained from V_{\max} data. Sabot *et al.* (2020) tested the hypothesis that k_{\max} should reflect long-term site climate (both average and extreme conditions). Whilst their results tended to support this link to long-term climate, high variability in derived k_{\max} estimates at moderate MAP ranges (i.e. 700–800 mm yr⁻¹) implies that further research is still needed. In all likelihood diversity in k_{\max} simply reflects a further axis by which hydraulic strategies trade off between and among species. Nevertheless, deriving k_{\max} as Sabot *et al.* (2020) did, is likely to reflect a more realistic route forwards than simply assuming fixed values, as we did in this study. A further option might be to leverage recent efforts to link VOD to vegetation water content (Liu *et al.*, 2021b), utilising this decadal timeseries to determine k_{\max} . Unfortunately microwave-derived estimates of VOD are extremely coarse (please refer to Fig. 7) and their interpretation is hindered by changes in leaf wetness (Xu *et al.*, 2021) and canopy biomass (Momen *et al.*, 2017). This may make it hard to relate directly to individual species but may work adequately for coarser vegetation simulations.

Role of cuticular conductance, g_{\min}

Choat *et al.* (2018) argued that evaporative loss via cuticular conductance was an important control point in the pathway of plants towards hydraulic failure. Although an earlier study with CABLE incorporated g_{\min} in the hydraulics implementation (De Kauwe *et al.*, 2020), we did not use this here for two reasons. First, it

represents a further parameter to determine for each species. The values used by De Kauwe *et al.* (2020) ranged from 0.25 to 0.8 mmol m⁻² s⁻¹, implying that fixing the value across species was not straightforward. As noted above, the impact of g_{\min} across the more arid regions in the earlier study (De Kauwe *et al.*, 2020) was significant and may have been overstated (too high a g_{\min}). Further data to inform model parameterisation of g_{\min} are much needed and may be aided by recent advances (Márquez *et al.*, 2022). Second, as our simulations have demonstrated, the profit maximisation already simulates very negative Ψ_{\min} values in extreme drought. Consequently, there is likely to be limited sensitivity to the role of g_{\min} in this model compared with a stomatal model that more strongly attenuates evaporation as root-zone water becomes limiting. Future work that revisits the degree of stomatal control in optimal stomatal models is perhaps needed first before connections are made to g_{\min} . Nevertheless, given the physiological importance of g_{\min} to predicting drought mortality, this is a key future avenue of research.

Future directions

In this study, we explored resilience to drought by using a bottom-up approach to integrate traits and climate to gain insight into species vulnerability across their distribution. However, drought susceptibility also varies within a species (Tuomela, 1997; Taeger *et al.*, 2013), which is a key axis of variation that we are unable to currently capture with modelling, severely limiting our predictive capacity as the climate changes. Although several compilations of physiological and hydraulic traits exist (Choat *et al.*, 2012; Martin-StPaul *et al.*, 2017; Liu *et al.*, 2019; Falster *et al.*, 2021; Peters *et al.*, 2021), few adequately sample variations within species across the environments they occupy (Rowland *et al.*, 2021; Trugman *et al.*, 2021). In the absence of direct observations of interspecific trait variation, modelling approaches that explore trait sensitivity (De Kauwe *et al.*, 2020; Papastefanou *et al.*, 2020) offer one possibility to bridge this gap. Nevertheless, these approaches are unlikely to capture important strategy trade-offs and their link to climate of origin. Alternatively, Konings & Gentine (2017) demonstrated that spatial variations in isohydricity could be derived from microwave estimates of vegetation water content. Conceivably these data may offer a pathway to better capture inter- and intraspecific variation in drought responses at the ecosystem scale, directly relevant to global models (please refer to also Konings *et al.* (2021) for a review). Nevertheless, microwave estimates are coarse (> 25 km), hampering comparison with field-based hydraulic traits; therefore, if used to parameterise models, we could run the risk of conflating within-species vs among-species drought risk.

Acknowledgements











MGDK, MEBS, AJP and AMU acknowledge support from the Australian Research Council (ARC) Centre of Excellence for Climate Extremes (CE170100023). MGDK, PM, LC, SR and AJP acknowledge support from the ARC Discovery Grant (DP190101823). MGDK was also supported from the NSW

Research Attraction and Acceleration Program and acknowledge support from Eucalypt Australia. MEBS acknowledges support from the UNSW Scientia PhD Scholarship Scheme. BEM acknowledges support from the ARC Laureate Fellowship FL190100003. AMU was supported by the ARC Discovery Early Career Researcher Award (DE200100086). We thank Stuart Allen for helping collate species distribution maps. We also thank Bristol's High Performance Computing cluster (Blue Crystal 4) and the National Computational Infrastructure at the Australian National University, an initiative of the Australian Government, for access to supercomputer resources. All data analysis and plots were generated using the PYTHON language and the Matplotlib library. We acknowledge the Editor, Dr Henry Adams and the two anonymous reviewers for their constructive comments.

Author contributions

MGDK designed the research in consultation with BEM, AJP, PM and LAC. MGDK and MEBS developed and implemented the model. RVG generated species distribution maps. AU calculated the precipitation drought metrics. SWR processed the satellite data. MGDK and MEBS collected species traits with input from BC. MGDK carried out all the analysis and wrote the original manuscript draft. All authors contributed to reviewing and editing the final manuscript.

ORCID

Lucas A. Cernusak  <https://orcid.org/0000-0002-7575-5526>
 Brendan Choat  <https://orcid.org/0000-0002-9105-640X>
 Martin G. De Kauwe  <https://orcid.org/0000-0002-3399-9098>
 Rachael V. Gallagher  <https://orcid.org/0000-0002-4680-8115>
 Belinda E. Medlyn  <https://orcid.org/0000-0001-5728-9827>
 Patrick Meir  <https://orcid.org/0000-0002-2362-0398>
 Andrew J. Pitman  <https://orcid.org/0000-0003-0604-3274>
 Sami W. Rifai  <https://orcid.org/0000-0003-3400-8601>
 Manon E. B. Sabot  <https://orcid.org/0000-0002-9440-4553>
 Anna M. Ukkola  <https://orcid.org/0000-0003-1207-3146>

Data availability

The model source code can be accessed freely after registration at <https://trac.nci.org.au/trac/cable>. In this paper we used CABLE revision 8740. All analysis code is freely available from: https://github.com/mdekauwe/SE_AUS_future_drought_risk_paper.git.

References

- Abram NJ, Henley BJ, Sen Gupta A, Lippmann TJR, Clarke H, Dowdy AJ, Sharples JJ, Nolan RH, Zhang T, Wooster MJ *et al.* 2021. Connections of climate change and variability to large and extreme forest fires in southeast Australia. *Communications Earth & Environment* 2: 8.
 Alexander LV, Arblaster JM. 2017. Historical and projected trends in temperature and precipitation extremes in Australia in observations and CMIP5. *Weather and Climate Extremes* 15: 34–56.

- Allen CD, Breshears DD, McDowell NG. 2015. On underestimation of global vulnerability to tree mortality and forest die-off from hotter drought in the Anthropocene. *Ecosphere* 6: art129.
- Anderegg LDL, Griffith DM, Cavender-Bares J, Riley WJ, Berry JA, Dawson TE, Still CJ. 2022. Representing plant diversity in land models: an evolutionary approach to make 'Functional Types' more functional. *Global Change Biology* 28: 2541–2554.
- Anderegg WRL, Flint A, Huang C, Flint L, Berry JA, Davis FW, Sperry JS, Field CB. 2015. Tree mortality predicted from drought-induced vascular damage. *Nature Geoscience* 8: 367–371.
- Anderegg WRL, Kane JM, Anderegg LDL. 2013. Consequences of widespread tree mortality triggered by drought and temperature stress. *Nature Climate Change* 3: 30–36.
- Andrew SC, Mokany K, Falster DS, Wenk E, Wright IJ, Merow C, Adams V, Gallagher RV. 2021. Functional diversity of the Australian flora: strong links to species richness and climate. *Journal of Vegetation Science* 32: e13018.
- Barigah TS, Charrier O, Douris M, Bonhomme M, Herbet S, Améglio T, Fichot R, Brignolas F, Cochard H. 2013. Water stress-induced xylem hydraulic failure is a causal factor of tree mortality in beech and poplar. *Annals of Botany* 112: 1431–1437.
- Barotto AJ, Fernandez ME, Gyenge J, Meyra A, Martinez-Meier A, Monteoliva S. 2016. First insights into the functional role of vascentric tracheids and parenchyma in *Eucalyptus* species with solitary vessels: do they contribute to xylem efficiency or safety? *Tree Physiology* 36: 1485–1497.
- Bastos A, Orth R, Reichstein M, Ciais P, Viovy N, Zaehle S, Anthoni P, Arneth A, Gentile P, Joetzer E *et al.* 2021. Vulnerability of European ecosystems to two compound dry and hot summers in 2018 and 2019. *Earth System Dynamics* 12: 1015–1035.
- deBoer HJ, Drake PL, Wendt E, Price CA, Schulze E-D, Turner NC, Nicolle D, Veneklaas EJ. 2016. Apparent overinvestment in leaf venation relaxes leaf morphological constraints on photosynthesis in arid habitats. *Plant Physiology* 172: 2286–2299.
- Bonan GB, Williams M, Fisher RA, Oleson KW. 2014. Modeling stomatal conductance in the earth system: linking leaf water-use efficiency and water transport along the soil–plant–atmosphere continuum. *Geoscientific Model Development* 7: 2193–2222.
- Bourne AE, Creek D, Peters JMR, Ellsworth DS, Choat B. 2017. Species climate range influences hydraulic and stomatal traits in *Eucalyptus* species. *Annals of Botany* 120: 123–133.
- Brodribb TJ, Cochard H. 2009. Hydraulic failure defines the recovery and point of death in water-stressed conifers. *Plant Physiology* 149: 575–584.
- Bureau of Meteorology. 2020. *Special Climate Statement 70 update-drought conditions in Australia and impact on water resources in the Murray-Darling Basin*. Canberra, ACT, Australia: Commonwealth of Australia. [WWW document] URL <http://www.bom.gov.au/climate/current/statements/scs70.pdf> [accessed 29 March 2022].
- Campbell GS. 1974. A simple method for determining unsaturated conductivity from moisture retention data. *Soil Science* 117: 311–314.
- Cernusak LA, Hutley LB, Beringer J, Holtum JAM, Turner BL. 2011. Photosynthetic physiology of eucalypts along a sub-continental rainfall gradient in northern Australia. *Agricultural and Forest Meteorology* 151: 1462–1470.
- Choat B, Brodribb TJ, Brodersen CR, Duursma RA, López R, Medlyn BE. 2018. Triggers of tree mortality under drought. *Nature* 558: 531–539.
- Choat B, Jansen S, Brodribb TJ, Cochard H, Delzon S, Bhaskar R, Bucci SJ, Feild TS, Gleason SM, Hacke UG *et al.* 2012. Global convergence in the vulnerability of forests to drought. *Nature* 491: 752–755.
- Christina M, Nouvellon Y, Laclau J-P, Stape JL, Bouillet J-P, Lambais GR, leMaire G. 2017. Importance of deep water uptake in tropical eucalypt forest. *Functional Ecology* 31: 509–519.
- Clearwater MJ, Meinzer FC. 2001. Relationships between hydraulic architecture and leaf photosynthetic capacity in nitrogen-fertilized *Eucalyptus grandis* trees. *Tree Physiology* 21: 683–690.
- Cochard H, Pimont F, Ruffault J, Martin-StPaul N. 2021. SurEau: a mechanistic model of plant water relations under extreme drought. *Annals of Forest Science* 78: 55.
- Cook BI, Mankin JS, Anchukaitis KJ. 2018. Climate change and drought: from past to future. *Current Climate Change Reports* 4: 164–179.
- De Kauwe MG, Kala J, Lin Y-S, Pitman AJ, Medlyn BE, Duursma RA, Abramowitz G, Wang Y-P, Miralles DG. 2015b. A test of an optimal stomatal conductance scheme within the CABLE land surface model. *Geoscientific Model Development* 8: 431–452.
- De Kauwe MG, Medlyn BE, Ukkola AM, Mu M, Sabot MEB, Pitman AJ, Meir P, Cernusak LA, Rifai SW, Choat B *et al.* 2020. Identifying areas at risk of drought-induced tree mortality across South-Eastern Australia. *Global Change Biology* 26: 5716–5733.
- De Kauwe MG, Medlyn BE, Tissue DT. 2021. To what extent can rising [CO₂] ameliorate plant drought stress? *New Phytologist* 231: 2118–2124.
- De Kauwe MG, Zhou S-X, Medlyn BE, Pitman AJ, Wang Y-P, Duursma RA, Prentice IC. 2015a. Do land surface models need to include differential plant species responses to drought? Examining model predictions across a mesic-xeric gradient in Europe. *Biogeosciences* 12: 7503–7518.
- Decker M, Or D, Pitman A, Ukkola A. 2017. New turbulent resistance parameterization for soil evaporation based on a pore-scale model: impact on surface fluxes in CABLE. *Journal of Advances in Modeling Earth Systems* 9: 220–238.
- Dewar R, Mauranen A, Mäkelä A, Hölttä T, Medlyn B, Vesala T. 2018. New insights into the covariation of stomatal, mesophyll and hydraulic conductances from optimization models incorporating nonstomatal limitations to photosynthesis. *New Phytologist* 217: 571–585.
- Dietze MC, Fox A, Beck-Johnson LM, Betancourt JL, Hooten MB, Jarnevich CS, Keitt TH, Kenney MA, Laney CM, Larsen LG *et al.* 2018. Iterative near-term ecological forecasting: needs, opportunities, and challenges. *Proceedings of the National Academy of Sciences, USA* 115: 1424–1432.
- vanDijk AIJM, Beck HE, Crosbie RS, deJeu RAM, Liu YY, Podger GM, Timbal B, Viney NR. 2013. The Millennium Drought in southeast Australia (2001–2009): natural and human causes and implications for water resources, ecosystems, economy, and society: causes and impacts of Australia's record drought. *Water Resources Research* 49: 1040–1057.
- Du J, Kimball JS, Jones LA, Kim Y, Glassy J, Watts JD. 2017. A global satellite environmental data record derived from AMSR-E and AMSR2 microwave Earth observations. *Earth System Science Data* 9: 791–808.
- Duan H, Amthor JS, Duursma RA, O'Grady AP, Choat B, Tissue DT. 2013. Carbon dynamics of eucalypt seedlings exposed to progressive drought in elevated [CO₂] and elevated temperature. *Tree Physiology* 33: 779–792.
- Eller CB, Rowland L, Oliveira RS, Bittencourt PRL, Barros FV, da Costa ACL, Meir P, Friend AD, Mencuccini M, Sitch S *et al.* 2018. Modelling tropical forest responses to drought and El Niño with a stomatal optimization model based on xylem hydraulics. *Philosophical Transactions of the Royal Society of London. Series B: Biological Sciences* 373: 20170315.
- Eller CB, Rowland L, Mencuccini M, Rosas T, Williams K, Harper A, Medlyn BE, Wagner Y, Klein T, Teodoro GS *et al.* 2020. Stomatal optimization based on xylem hydraulics (SOX) improves land surface model simulation of vegetation responses to climate. *New Phytologist* 226: 1622–1637.
- Falster D, Gallagher R, Wenk E, Wright I, Indiarto D. 2021. AUSTRAITS – a curated plant trait database for the Australian flora. *Scientific Data* 8: 254.
- Farquhar GD, vonCaemmerer S, Berry JA. 1980. A biochemical model of photosynthetic CO₂ assimilation in leaves of C3 species. *Planta* 149: 78–90.
- Farquhar GD, Sharkey TD. 1982. Stomatal conductance and photosynthesis. *Annual Review of Plant Physiology* 33: 317–345.
- Franks PJ, Gibson A, Bachelard EP. 1995. Xylem permeability and embolism susceptibility in seedlings of *Eucalyptus camaldulensis* Dehnh. from two different climatic zones. *Functional Plant Biology* 22: 15–21.
- Friedlingstein P, O'Sullivan M, Jones MW, Andrew RM, Hauck J, Olsen A, Peters GP, Peters W, Pongratz J, Sitch S *et al.* 2020. Global carbon budget 2020. *Earth System Science Data* 12: 3269–3340.
- Ghannoum O, Phillips NG, Sears MA, Logan BA, Lewis JD, Conroy JP, Tissue DT. 2010. Photosynthetic responses of two eucalypts to industrial-age changes in atmospheric [CO₂] and temperature. *Plant, Cell & Environment* 33: 1671–1681.
- Grassi G, Meir P, Cromer R, Tompkins D, Jarvis PG. 2002. Photosynthetic parameters in seedlings of *Eucalyptus grandis* as affected by rate of nitrogen supply. *Plant, Cell & Environment* 25: 1677–1688.

- Green JK, Seneviratne SI, Berg AM, Findell KL, Hagemann S, Lawrence DM, Gentine P. 2019. Large influence of soil moisture on long-term terrestrial carbon uptake. *Nature* 565: 476–479.
- Grose MR, Narsey S, Delage FP, Dowdy AJ, Bador M, Boschat G, Chung C, Kajtar JB, Rauniyar S, Freund MB *et al.* 2020. Insights from CMIP6 for Australia's future climate. *Earth's Future* 8: e2019EF001469.
- Hammond WM, Yu K, Wilson LA, Will RE, Anderegg WRL, Adams HD. 2019. Dead or dying? Quantifying the point of no return from hydraulic failure in drought-induced tree mortality. *New Phytologist* 223: 1834–1843.
- Haverd V, Smith B, Nieradzki LP, Briggs PR. 2014. A stand-alone tree demography and landscape structure module for Earth system models: integration with inventory data from temperate and boreal forests. *Biogeosciences* 11: 4039–4055.
- Haverd V, Smith B, Nieradzki L, Briggs PR, Woodgate W, Trudinger CM, Canadell JG, Cuntz M. 2018. A new version of the CABLE land surface model (Subversion revision r4601) incorporating land use and land cover change, woody vegetation demography, and a novel optimisation-based approach to plant coordination of photosynthesis. *Geoscientific Model Development* 11: 2995–3026.
- Hengl T, Mendes de Jesus J, Heuvelink GBM, Ruiperez Gonzalez M, Kilibarda M, Blagotić A, Shangguan W, Wright MN, Geng X, Bauer-Marschallinger B *et al.* 2017. SoilGrids250m: global gridded soil information based on machine learning. *PLoS ONE* 12: e0169748.
- Huang Z, Xu Z, Blumfield TJ, Bubb K. 2008. Variations in relative stomatal and biochemical limitations to photosynthesis in a young blackbutt (*Eucalyptus pilularis*) plantation subjected to different weed control regimes. *Tree Physiology* 28: 997–1005.
- Humphrey V, Berg A, Ciais P, Gentine P, Jung M, Reichstein M, Seneviratne SI, Frankenberg C. 2021. Soil moisture-atmosphere feedback dominates land carbon uptake variability. *Nature* 592: 65–69.
- Jones D, Wang W, Fawcett R. 2009. High-quality spatial climate data-sets for Australia. *Australian Meteorological and Oceanographic Journal* 58: 233–248.
- Julio Camarero J, Gazol A, Sangüesa-Barreda G, Cantero A, Sánchez-Salguero R, Sánchez-Miranda A, Granda E, Serra-Maluquer X, Ibáñez R. 2018. Forest growth responses to drought at short- and long-term Scales in Spain: squeezing the stress memory from tree rings. *Frontiers in Ecology and Evolution* 6: 9.
- Keenan T, Sabate S, Gracia C. 2010. The importance of mesophyll conductance in regulating forest ecosystem productivity during drought periods. *Global Change Biology* 16: 1019–1034.
- Kennedy D, Swenson S, Oleson KW, Lawrence DM, Fisher R, Lola da Costa AC, Gentine P. 2019. Implementing plant hydraulics in the community land model, v.5. *Journal of Advances in Modeling Earth Systems* 11: 485–513.
- Konings AG, Gentine P. 2017. Global variations in ecosystem-scale isohydricity. *Global Change Biology* 23: 891–905.
- Konings AG, Saatchi SS, Frankenberg C, Keller M, Leshyk V, Anderegg WRL, Humphrey V, Matheny AM, Trugman A, Sack L *et al.* 2021. Detecting forest response to droughts with global observations of vegetation water content. *Global Change Biology* 27: 6005–6024.
- Kowalczyk EA, Wang YP, Law RM, Davies HL, McGregor JL, Abramowitz GS. 2006. *The CSIRO Atmosphere Biosphere Land Exchange (CABLE) model for use in climate models and as an offline model*. Aspendale, Vic., Australia: CSIRO Marine, Atmospheric Research.
- Leuning R, Cromer RN, Rance S. 1991. Spatial distributions of foliar nitrogen and phosphorus in crowns of *Eucalyptus grandis*. *Oecologia* 88: 504–510.
- Li S, Feifel M, Karimi Z, Schuldt B, Choat B, Jansen S. 2015. Leaf gas exchange performance and the lethal water potential of five European species during drought. *Tree Physiology* 36: 179–192.
- Li X, Blackman CJ, Choat B, Duursma RA, Rymer PD, Medlyn BE, Tissue DT. 2018. Tree hydraulic traits are coordinated and strongly linked to climate-of-origin across a rainfall gradient. *Plant, Cell & Environment* 41: 646–660. [Correction added after first publication 22 April 2022: reference has been corrected.]
- Liu H, Gleason SM, Hao G, Hua L, He P, Goldstein G, Ye Q. 2019. Hydraulic traits are coordinated with maximum plant height at the global scale. *Science Advances* 5: eaav1332.
- Liu Y, Holtzman NM, Konings AG. 2021a. Global ecosystem-scale plant hydraulic traits retrieved using model–data fusion. *Hydrology and Earth System Sciences* 25: 2399–2417.
- Liu Y, Konings AG, Kennedy D, Gentine P. 2021b. Global coordination in plant physiological and rooting strategies in response to water stress. *Global Biogeochemical Cycles* 35: 1–23.
- Lorenz R, Pitman AJ, Donat MG, Hirsch AL, Kala J, Kowalczyk EA, Law RM, Srbinovsky J. 2014. Representation of climate extreme indices in the ACCESS1.3b coupled atmosphere–land surface model. *Geoscientific Model Development* 7: 545–567.
- van Mantgem PJ, Stephenson NL, Byrne JC, Daniels LD, Franklin JF, Fulé PJ, Harmon ME, Larson AJ, Smith JM, Taylor AH *et al.* 2009. Widespread increase of tree mortality rates in the Western United States. *Science* 323: 521–524.
- Márquez DA, Stuart-Williams H, Farquhar GD, Busch FA. 2022. Cuticular conductance of adaxial and abaxial leaf surfaces and its relation to minimum leaf surface conductance. *New Phytologist* 233: 156–168.
- Martin-StPaul N, Delzon S, Cochard H. 2017. Plant resistance to drought depends on timely stomatal closure. *Ecology Letters* 20: 1437–1447.
- McDowell N, Pockman WT, Allen CD, Breshears DD, Cobb N, Kolb T, Plaut J, Sperry J, West A, Williams DG *et al.* 2008. Mechanisms of plant survival and mortality during drought: why do some plants survive while others succumb to drought? *New Phytologist* 178: 719–739.
- McDowell NG, Williams AP, Xu C, Pockman WT, Dickman LT, Sevanto S, Pangle R, Limousin J, Plaut J, Mackay DS *et al.* 2016. Multi-scale predictions of massive conifer mortality due to chronic temperature rise. *Nature Climate Change* 6: 295–300.
- McKee TB, Doesken NJ, Kleist J. 1993. The relation of drought frequency and duration to time scales. In: *Proceedings of the 8th conference on applied climatology, Anaheim, California, 17–22 January 1993*, 179–184.
- McVicar TR. 2011. *Near-surface wind speed (CSIRO)*, v.10. Data collection. doi: 10.25919/5c5106acbc02.
- McVicar TR, Van Niel TG, Li LT, Roderick ML, Rayner DP, Ricciardulli L, Donohue RJ. 2008. Wind speed climatology and trends for Australia, 1975–2006: capturing the stilling phenomenon and comparison with near-surface reanalysis output. *Geophysical Research Letters* 35: L20403.
- Medlyn BE, Barton CVM, Broadmeadow MSJ, Ceulemans R, Angelis PD, Forstreuter M, Freeman M, Jackson SB, Kellomäki S, Laita E *et al.* 2001. Stomatal conductance of forest species after long-term exposure to elevated CO₂ concentration: a synthesis. *New Phytologist* 149: 247–264.
- Mitchell PJ, O'Grady AP, Hayes KR, Pinkard EA. 2014. Exposure of trees to drought-induced die-off is defined by a common climatic threshold across different vegetation types. *Ecology and Evolution* 4: 1088–1101.
- Momen M, Wood JD, Novick KA, Pangle R, Pockman WT, McDowell NG, Konings AG. 2017. Interacting effects of leaf water potential and biomass on vegetation optical depth. *Journal of Geophysical Research: Biogeosciences* 122: 3031–3046.
- Mu M, De Kauwe MG, Ukkola AM, Pitman AJ, Guo W, Hobeichi S, Briggs PR. 2021. Exploring how groundwater buffers the influence of heatwaves on vegetation function during multi-year droughts. *Earth System Dynamics* 12: 919–938.
- Mueller B, Seneviratne SI. 2012. Hot days induced by precipitation deficits at the global scale. *Proceedings of the National Academy of Sciences, USA* 109: 12398–12403.
- Nepstad DC, Tohver IM, Ray D, Moutinho P, Cardinot G. 2007. Mortality of large trees and lianas following experimental drought in an Amazon forest. *Ecology* 88: 2259–2269.
- Neufeld HS, Grantz DA, Meinzer FC, Goldstein G, Crisosto GM, Crisosto C. 1992. Genotypic variability in vulnerability of leaf xylem to cavitation in water-stressed and well-irrigated sugarcane. *Plant Physiology* 100: 1020–1028.
- Nolan RH, Boer MM, Collins L, Resco de Dios V, Clarke H, Jenkins M, Kenny B, Bradstock RA. 2020. Causes and consequences of eastern Australia's 2019–20 season of mega-fires. *Global Change Biology* 26: 1039–1041.
- Nolan RH, Gauthey A, Losso A, Medlyn BE, Smith R, Chhajed SS, Fuller K, Song M, Li X, Beaumont LJ *et al.* 2021. Hydraulic failure and tree size linked with canopy die-back in eucalypt forest during extreme drought. *New Phytologist* 230: 1354–1365.
- Papastefanou P, Zang CS, Pugh TAM, Liu D, Grams TEE, Hickler T, Rammig A. 2020. A dynamic model for strategies and dynamics of plant water-potential regulation under drought conditions. *Frontiers in Plant Science* 11: 373.

- Peng C, Ma Z, Lei X, Zhu Q, Chen H, Wang W, Liu S, Li W, Fang X, Zhou X. 2011. A drought-induced pervasive increase in tree mortality across Canada's boreal forests. *Nature Climate Change* 1: 467–471.
- Peters JMR, López R, Nolf M, Hutley LB, Wardlaw T, Cernusak LA, Choat B. 2021. Living on the edge: a continental-scale assessment of forest vulnerability to drought. *Global Change Biology* 27: 3620–3641.
- Petit-Cailleux C, Davi H, Lefèvre F, Verkerk PJ, Fady B, Lindner M, Oddou-Muratorio S. 2021. Tree mortality risks under climate change in Europe: assessment of silviculture practices and genetic conservation networks. *Frontiers in Ecology and Evolution* 9: 706414.
- Pitman AJ, Avila FB, Abramowitz G, Wang YP, Phipps SJ, deNoblet-Ducoudré N. 2011. Importance of background climate in determining impact of land-cover change on regional climate. *Nature Climate Change* 1: 472–475.
- Pivovarov AL, McDowell NG, Rodrigues TB, Brodribb T, Cernusak LA, Choat B, Grossiord C, Ishida Y, Jardine KJ, Laurance S *et al.* 2021. Stability of tropical forest tree carbon-water relations in a rainfall exclusion treatment through shifts in effective water uptake depth. *Global Change Biology* 27: 6454–6466.
- Raupach MR. 1994. Simplified expressions for vegetation roughness length and zero-plane displacement as functions of canopy height and area index. *Boundary-Layer Meteorology* 71: 211–216.
- Raupach MR, Finkel K, Zhang L. 1997. *SCAM (soil-canopy-atmosphere model): description and comparison with field data*. Aspendale, Vic., Australia: CSIRO CEM Technical Report: 81.
- Reichstein M, Bahn M, Ciais P, Frank D, Mahecha MD, Seneviratne SI, Zscheischler J, Beer C, Buchmann N, Frank DC *et al.* 2013. Climate extremes and the carbon cycle. *Nature* 500: 287–295.
- Renner IW, Elith J, Baddeley A, Fithian W, Hastie T, Phillips SJ, Popovic G, Warton DI. 2015. Point process models for presence-only analysis. *Methods in Ecology and Evolution* 6: 366–379.
- Ridder NN, Pitman AJ, Westra S, Ukkola A, Do HX, Bador M, Hirsch AL, Evans JP, Di Luca A, Zscheischler J. 2020. Global hotspots for the occurrence of compound events. *Nature Communications* 11: 5956.
- Rifai SW, De Kauwe MG, Ukkola AM, Cernusak LA, Meir P, Medlyn BE, Pitman AJ. 2021. Thirty-eight years of CO₂ fertilization have outpaced growing aridity to drive greening of Australian woody ecosystems. *Biogeosciences* 19: 491–515.
- Rowland L, da Costa ACL, Galbraith DR, Oliveira RS, Binks OJ, Oliveira AAR, Pullen AM, Doughty CE, Metcalfe DB, Vasconcelos SS *et al.* 2015. Death from drought in tropical forests is triggered by hydraulics not carbon starvation. *Nature* 528: 119–122.
- Rowland L, Oliveira RS, Bittencourt PRL, Giles AL, Coughlin I, Costa PDB, Domingues T, Ferreira LV, Vasconcelos SS, Junior JAS *et al.* 2021. Plant traits controlling growth change in response to a drier climate. *New Phytologist* 229: 1363–1374.
- Ruehr NK, Grote R, Mayr S, Arneth A. 2019. Beyond the extreme: recovery of carbon and water relations in woody plants following heat and drought stress. *Tree Physiology* 39: 1285–1299.
- Sabot MEB, De Kauwe MG, Pitman AJ, Medlyn BE, Verhoef A, Ukkola AM, Abramowitz G. 2020. Plant profit maximization improves predictions of European forest responses to drought. *New Phytologist* 226: 1638–1655.
- Sabot MEB, Kauwe MG, Pitman AJ, Medlyn BE, Ellsworth DS, Martin-StPaul N, Wu J, Choat B, Limousin J-M, Mitchell PJ *et al.* 2022. One stomatal model to rule them all? Towards improved representation of carbon and water exchange in global models. *Journal of Advances in Modeling Earth Systems* 14: e2021MS002761.
- Scharnweber T, Smiljanic M, Cruz-García R, Manthey M, Wilmking M. 2020. Tree growth at the end of the 21st century – the extreme years 2018/19 as template for future growth conditions. *Environmental Research Letters* 15: 74022.
- Slik JWF. 2004. El Niño droughts and their effects on tree species composition and diversity in tropical rain forests. *Oecologia* 141: 114–120.
- Slot M, Nardwattanawong T, Hernández GG, Bueno A, Riederer M, Winter K. 2021. Large differences in leaf cuticle conductance and its temperature response among 24 tropical tree species from across a rainfall gradient. *New Phytologist* 232: 1618–1631.
- Sperry JS, Venturas MD, Anderegg WRL, Mencuccini M, Mackay DS, Wang Y, Love DM. 2017. Predicting stomatal responses to the environment from the optimization of photosynthetic gain and hydraulic cost: a stomatal optimization model. *Plant, Cell & Environment* 40: 816–830.
- Sperry JS, Venturas MD, Todd HN, Trugman AT, Anderegg WRL, Wang Y, Tai X. 2019. The impact of rising CO₂ and acclimation on the response of US forests to global warming. *Proceedings of the National Academy of Sciences, USA* 116: 25734–25744.
- Swann ALS, Laguë MM, Garcia ES, Field JP, Breshears DD, Moore DJP, Saleska SR, Stark SC, Villegas JC, Law DJ *et al.* 2018. Continental-scale consequences of tree die-offs in North America: identifying where forest loss matters most. *Environmental Research Letters* 13: 55014.
- Taeger S, Fussi B, Konnerth M, Menzel A. 2013. Large-scale genetic structure and drought-induced effects on European Scots pine (*Pinus sylvestris* L.) seedlings. *European Journal of Forest Research* 132: 481–496.
- Teckentrup L, De Kauwe MG, Pitman AJ, Goll DS, Haverd V, Jain AK, Joetzier E, Kato E, Lienert S, Lombardozzi D *et al.* 2021. Assessing the representation of the Australian carbon cycle in global vegetation models. *Biogeosciences* 18: 5639–5668.
- Trowbridge AM, Adams HD, Collins A, Dickman LT, Grossiord C, Hoffland M, Malone S, Weaver DK, Sevanto S, Stoy PC *et al.* 2021. Hotter droughts alter resource allocation to chemical defenses in piñon pine. *Oecologia* 197: 921–938.
- Trugman AT, Anderegg LDL, Anderegg WRL, Das AJ, Stephenson NL. 2021. Why is tree drought mortality so hard to predict? *Trends in Ecology & Evolution* 36: 520–532.
- Trugman AT, Medvigy D, Mankin JS, Anderegg WRL. 2018. Soil moisture stress as a major driver of carbon cycle uncertainty. *Geophysical Research Letters* 45: 6495–6503.
- Tuomela K. 1997. Leaf water relations in six provenances of *Eucalyptus microtheca*: a greenhouse experiment. *Forest Ecology and Management* 92: 1–10.
- Ukkola AM, De Kauwe MG, Pitman AJ, Best MJ, Abramowitz G, Haverd V, Decker M, Houghton N. 2016a. Land surface models systematically overestimate the intensity, duration and magnitude of seasonal-scale evaporative droughts. *Environmental Research Letters* 11: 104012.
- Ukkola AM, De Kauwe MG, Roderick ML, Abramowitz G, Pitman AJ. 2020. Robust future changes in meteorological drought in CMIP6 projections despite uncertainty in precipitation. *Geophysical Research Letters* 46: e2020GL087820.
- Ukkola AM, Pitman AJ, Decker M, De Kauwe MG, Abramowitz G, Kala J, Wang Y-P. 2016b. Modelling evapotranspiration during precipitation deficits: identifying critical processes in a land surface model. *Hydrology and Earth System Sciences* 20: 2403–2419.
- Venturas MD, Sperry JS, Love DM, Frehner EH, Allred MG, Wang Y, Anderegg WRL. 2018. A stomatal control model based on optimization of carbon gain versus hydraulic risk predicts aspen sapling responses to drought. *New Phytologist* 220: 836–850.
- Wang YP, Kowalczyk E, Leuning R, Abramowitz G, Raupach MR, Pak B, vanGorsel E, Luhar A. 2011. Diagnosing errors in a land surface model (CABLE) in the time and frequency domains. *Journal of Geophysical Research* 116: G01034.
- Wang YP, Law RM, Pak B. 2010. A global model of carbon, nitrogen and phosphorus cycles for the terrestrial biosphere. *Biogeosciences* 7: 2261–2282.
- Wang Y-P, Leuning R. 1998. A two-leaf model for canopy conductance, photosynthesis and partitioning of available energy I: model description and comparison with a multi-layered model. *Agricultural and Forest Meteorology* 91: 89–111.
- Warren C. 2004. Evergreen trees do not maximize instantaneous photosynthesis. *Trends in Plant Science* 9: 270–274.
- Warren CR. 2004. The photosynthetic limitation posed by internal conductance to CO₂ movement is increased by nutrient supply. *Journal of Experimental Botany* 55: 2313–2321.
- Williams AP, Cook ER, Smerdon JE, Cook BI, Abatzoglou JT, Bolles K, Baek SH, Badger AM, Livneh B. 2020. Large contribution from anthropogenic warming to an emerging North American megadrought. *Science* 368: 314–318.
- Williams M, Law BE, Anthoni PM, Unsworth MH. 2001. Use of a simulation model and ecosystem flux data to examine carbon-water interactions in ponderosa pine. *Tree Physiology* 21: 287–298.

- Wolf A, Anderegg WRL, Pacala SW. 2016. Optimal stomatal behavior with competition for water and risk of hydraulic impairment. *Proceedings of the National Academy of Sciences, USA* 113: E7222–E7230.
- Xu X, Konings AG, Longo M, Feldman A, Xu L, Saatchi S, Wu D, Wu J, Moorcroft P. 2021. Leaf surface water, not plant water stress, drives diurnal variation in tropical forest canopy water content. *New Phytologist* 231: 122–136.
- Xu X, Medvigy D, Powers JS, Becknell JM, Guan K. 2016. Diversity in plant hydraulic traits explains seasonal and inter-annual variations of vegetation dynamics in seasonally dry tropical forests. *New Phytologist* 212: 80–95.
- Yang J, Duursma RA, De Kauwe MG, Kumarathunge D, Jiang M, Mahmud K, Gimeno TE, Crous KY, Ellsworth DS, Peters J *et al.* 2019. Incorporating non-stomatal limitation improves the performance of leaf and canopy models at high vapour pressure deficit. *Tree Physiology* 39: 1961–1974.
- Yang J, Medlyn BE, De Kauwe MG, Duursma RA. 2018. Applying the concept of ecohydrological equilibrium to predict steady state leaf area index. *Journal of Advances in Modeling Earth Systems* 10: 1740–1758.
- Zhou S, Duursma RA, Medlyn BE, Kelly JW, Prentice IC. 2013. How should we model plant responses to drought? An analysis of stomatal and non-stomatal responses to water stress. *Agricultural and Forest Meteorology* 182–183: 204–214.
- Zhou S-X, Medlyn BE, Prentice IC. 2016. Long-term water stress leads to acclimation of drought sensitivity of photosynthetic capacity in xeric but not riparian *Eucalyptus* species. *Annals of Botany* 117: 133–144.
- Zolfaghari S, Villalobos-Vega R, Zeppel M, Cleverly J, Rumman R, Hingee M, Boulain N, Li Z, Eamus D. 2017. Transpiration of *Eucalyptus* woodlands across a natural gradient of depth-to-groundwater. *Tree Physiology* 37: 961–975.
- Zscheischler J, Michalak AM, Schwalm C, Mahecha MD, Huntzinger DN, Reichstein M, Berthier G, Ciais P, Cook RB, El-Masri B *et al.* 2014. Impact of large-scale climate extremes on biospheric carbon fluxes: an intercomparison based on M5TMIP data. *Global Biogeochemical Cycles* 28: 585–600.

Supporting Information

Additional Supporting Information may be found online in the Supporting Information section at the end of the article.

Fig. S1 South-Eastern Australia's rainfall deciles for January 2017 to August 2019.

Fig. S2 A comparison between fluxes simulated by CABLE with (hydraulics) and without (Control) the plant hydraulics module for gross primary productivity (GPP) and latent heat flux (LE) at the Tumberumba fluxnet site during a pronounced period of water stress.

Fig. S3 A comparison between fluxes simulated by CABLE with (hydraulics) and without (Control) the plant hydraulics module for gross primary productivity (GPP) and latent heat flux (LE) at the Wombat State Forest fluxnet site during a pronounced period of water stress.

Fig. S4 A comparison between fluxes simulated by CABLE with (hydraulics) and without (Control) the plant hydraulics module for gross primary productivity (GPP) and latent heat flux (LE) at the Whroo fluxnet site during a pronounced period of water stress.

Fig. S5 Maps showing the minimum leaf water potential (μ_{min}) simulated by CABLE during the drought (CTL: 2017–2019).

Fig. S6 Maps showing the minimum leaf water potential (μ_{min}) simulated by CABLE during the drought with a 20% reduction in rainfall (rPPT: 2017–2019).

Fig. S7 Maps showing the minimum leaf water potential (μ_{min}) simulated by CABLE during the drought with a 20% reduction in rainfall and a doubling of the atmospheric carbon dioxide concentration ($\text{eCO}_2 \times \text{rPPT}$: 2017–2019).

Fig. S8 Maps showing the maximum percentage loss of hydraulic conductivity (%) simulated by CABLE during the drought (2017–2019), rPPT experiment.

Fig. S9 Maps showing the maximum percentage loss of hydraulic conductivity (%) simulated by CABLE during the drought (2017–2019), $\text{eCO}_2 \times \text{rPPT}$ experiment.

Fig. S10 Maps showing the relative maximum percentage loss of hydraulic conductivity (%) simulated by CABLE when the maximum hydraulic conductance in the soil–plant continuum (k_{max}) is halved for the 2017–2019 drought (rPPT experiment).

Fig. S11 Maps showing the relative maximum percentage loss of hydraulic conductivity (%) simulated by CABLE when the maximum hydraulic conductance in the soil–plant continuum (k_{max}) is halved for the 2017–2019 drought ($\text{eCO}_2 \times \text{rPPT}$ experiment).

Methods S1 Site validation of CABLE at Ozflux sites.

Please note: Wiley Blackwell are not responsible for the content or functionality of any Supporting Information supplied by the authors. Any queries (other than missing material) should be directed to the *New Phytologist* Central Office.